



MASTERARBEIT / MASTER'S THESIS

Titel der Masterarbeit / Title of the Master's Thesis

„Chromosome Configuration of Oral Cavity Symbionts“

verfasst von / submitted by

Nicole Catherina Krause, BSc

angestrebter akademischer Grad / in partial fulfilment of the requirements for the degree of
Master of Science (MSc)

Wien, 2022 / Vienna, 2022

Studienkennzahl lt. Studienblatt /
degree programme code as it appears on
the student record sheet:

UA 066 830

Studienrichtung lt. Studienblatt /
degree programme as it appears on
the student record sheet:

Masterstudium Molekulare Mikrobiologie,
Mikrobielle Ökologie und Immunbiologie

Betreut von / Supervisor:

Assoz. Prof. Dr. Silvia Bulgheresi,
Privatdoz.

Table of Contents

<i>Abstract</i>	7
<i>German Abstract</i>	8
<i>Introduction</i>	9
Symbiosis	9
Human Microbiome	10
Human Oral Microbiome	10
Adhesive Fimbriae	11
Multicellular Bacteria	12
Rod-shaped Bacterial Reproduction	12
Longitudinally Dividing Bacteria	13
Bacterial Chromatin	14
Chromosome Configuration	15
<i>E. coli</i> Chromosome Segregation	16
ParABS-Mediated Chromosome Segregation	17
<i>A. filiformis</i> , <i>S. muelleri</i> , <i>C. steedae</i>	18
<i>Aim</i>	20
<i>Methods</i>	21
<i>A. filiformis</i> , <i>S. muelleri</i> and <i>C. steedae</i> strains and cultivation	21
qPCR	22
Morphometric measurements	26
Western Blotting	26
Immunostaining	27
Fluorescence in-situ hybridization	28
Microscopy and analysis	34
<i>Results</i>	35
Cell quantification of <i>A. filiformis</i>	35
Morphometric Measurements	39
DNA localization in <i>S. muelleri</i> and <i>C. steedae</i> may be polar	40
Detection of the tubulin homolog FtsZ was unsuccessful	41
<i>C. steedae</i> fimbriae localization is polar	42
<i>Ori</i> are polar and <i>ter</i> are found at mid-cell in <i>S. muelleri</i>	43
<i>Ori</i> is polar and <i>ter</i> is found at mid-cell in <i>C. steedae</i>	45
<i>C. steedae</i> plasmid localizes to the middle of the cell	48
<i>Discussion</i>	49
Cell quantification	49

Morphometric measurements _____	50
Optimization of immunostaining protocol for FtsZ _____	51
<i>C. steedae</i> and <i>S. muelleri</i> fimbriae and DNA localization are polar _____	52
<i>S. muelleri</i> has a fixed chromosome configuration (<i>ori-ter-ter-ori</i>) _____	53
<i>C. steedae</i> has a fixed chromosome configuration (<i>ori-ter-ter-ori</i>) _____	53
Diploidy _____	54
Fixed chromosome configuration _____	55
<i>C. steedae</i> plasmid is excluded from the poles _____	56
<i>Concluding remarks</i> _____	57
<i>Outlook</i> _____	60
<i>References</i> _____	61

Table of Figures

Figure 1. Chromosome configuration of <i>A. filiformis</i> , <i>Ca. T. hypermnestrae</i> and <i>Ca. T. oneisti</i>	16
Figure 1. <i>E. coli</i> chromosome segregation.....	17
Figure 3. Phase-contrast microscopy images of <i>A. filiformis</i> , <i>S. muelleri</i> and <i>C. steedae</i>	19
Figure 2. <i>S. muelleri</i> and <i>C. steedae</i> chromosome maps.....	28
Figure 5. OD ₆₀₀ vs DNA quantity.....	35
Figure 6. <i>gyrB</i> standards and samples.....	36
Figure 7. <i>rpoB</i> standards and samples.....	36
Figure 8. Mean OD ₆₀₀ vs. copies per 1 ml of culture <i>gyrB</i>	37
Figure 3. Mean OD ₆₀₀ vs. copies per 1 ml of culture <i>rpoB</i>	39
Figure 10. DNA localization in <i>S. muelleri</i>	40
Figure 11. DNA localization in <i>C. steedae</i>	41
Figure 12. Western blot against FtsZ.....	42
Figure 13. Polarized fimbriae localization in <i>C. steedae</i>	43
Figure 14. <i>ori</i> FISH experiment in <i>S. muelleri</i>	44
Figure 4. <i>ter</i> FISH experiment in <i>S. muelleri</i>	45
Figure 16. <i>ori</i> FISH experiment in <i>C. steedae</i>	46
Figure 17. <i>ter</i> FISH experiment in <i>C. steedae</i>	47
Figure 18. Plasmid FISH experiment in <i>C. steedae</i>	48
Figure 19. Diagram showing proposed chromosome configuration in <i>S. muelleri</i> and <i>C. steedae</i> ..	54
Figure 20. Genome maps of <i>A. filiformis</i> , <i>S. muelleri</i> and <i>C. steedae</i>	58

Acknowledgements

I would like to greatly thank my supervisor Silvia Bulgheresi for welcoming me into her group and for her overwhelming support during the last year. Her wise insights and encouragement were driving factors in cultivating a collaborative environment in which I was able to vastly expand my scientific horizons.

I would also like to thank Philipp Weber and Tobias Viehböck for their constant positivity and willingness to help me no matter what. Their guidance and support allowed me to have fun but also learn a huge amount of new scientific and analytical skills.

Additionally, I would like to thank everyone else in the Archaea Biology and Ecogenomics Division for always being helpful, patient, and supportive.

Abstract

A. filiformis, *S. muelleri* and *C. steedae* are oral cavity symbionts that form multicellular filaments. They belong to the *Neisseriaceae* family and reside in the mouths of warm-blooded vertebrates, including humans. The chromosome configurations of one previously studied nematode symbiont and *A. filiformis* are host-polarized, leading to an increased interest in the chromosome biology of other symbiotic bacteria. Here, we found that the DNA of *S. muelleri* and *C. steedae* is either dispersed throughout the cell or localized towards both host-attached poles. We also demonstrated, through immunostaining, that the fimbriae of *C. steedae* are localized on the cell concave side. Furthermore, the 80 kB plasmid in *C. steedae* was present at mid-cell and absent from the two poles. Finally, through fluorescence *in-situ* hybridization, we determined that *S. muelleri* and *C. steedae* are both diploid and have a fixed chromosome configuration. Their origins of replication (*ori*) localize at the two host-attached poles and the termini of replication (*ter*) at mid-cell, independent of the cell cycle stage. This chromosome configuration is referred to as fixed *ori-ter-ter-ori*.

German Abstract

A. filiformis, *S. muelleri* und *C. steedae* sind Symbionten, die mehrzellige Filamente bilden und in Mundhöhlen vorkommen. Sie gehören zur Familie der *Neisseriaceae* und befinden sich in den Mündern von warmblütigen Wirbeltieren, einschließlich der von Menschen. Die Chromosomenkonfiguration von Nematoden-Symbionten und *A. filiformis* wurde bereits untersucht und stellte sich als wirtspolarisiert heraus, was das Interesse an der Chromosomenbiologie weiterer symbiotischer Bakterien weckte. Hier kamen wir zu dem Schluss, dass die DNA von *S. muelleri* und *C. steedae* entweder in der gesamten Zelle verteilt ist oder in Richtung beider wirtsgebundener Pole lokalisiert ist. Wir haben auch durch Immunfärbung gezeigt, dass sich die Fimbrien von *C. steedae* an der konkaven Seite der Zelle befinden. Auch lokalisierte das 80 kB-Plasmid in *C. steedae* in der Mitte der Zelle vorhanden und fehlte an den beiden Polen. Durch Fluoreszenz-*in-situ*-Hybridisierung kamen wir zum Schluss, dass *S. muelleri* und *C. steedae* zwei Chromosomen besitzen (Diploidie) und eine fixierte Chromosomenkonfiguration haben. Deren Replikationsursprünge (*ori*) befinden sich an den beiden wirtsgebundenen Polen und die Termini (*ter*) in der Mitte der Zelle, unabhängig vom Zellzyklusstadium. Diese Chromosomenkonfiguration bezeichnen wir als fixierte *ori-ter-ter-ori*.

Introduction

Symbiosis

Symbiosis can be defined as a prolonged interaction between two different species living in close physical association (Oulhen, Schulz & Carrier, 2016). Microorganisms diversified long before large multicellular organisms, whose complex anatomy comprises a variety of unique microhabitats, leading to constant intricate interaction (Moran, 2006). Consequently, a range of different types of symbiotic relationships evolved. Despite the variety of symbiotic relationships that exist, they always include a host partner and a symbiont partner(s).

Symbiotic relationships are categorized depending on the location of the symbiont, the nature of the interaction and their method of transmission. Endosymbionts survive within the host body, while ectosymbionts thrive on the surface of the host body (Douglas, 2009). There are two main types of symbiont transmission, horizontal and vertical; however, a mixed mode is also common. Horizontally transmitted symbiotic bacteria are taken up from the environment by each host generation (Chrostek et al., 2017), while vertically transmitted symbionts get transferred through the female germline (Russell, Chappell & Sullivan, 2019). The latter type of transmission results in hosts that undergo uninterrupted transmission with their symbiont partners and are usually unable to live apart from their symbionts and vice versa (Bright & Bulgheresi, 2010).

The nature of symbiotic relationships usually fits into one of three categories: mutualism, commensalism and parasitism. Mutualism refers to the benefit of both organisms due to the interaction. For example, legumes form symbiotic relationships with nitrogen-fixing soil bacteria known as rhizobia, allowing nodules to form on the plant root where the bacteria convert nitrogen into ammonia taken up by the plant (Wang, Liu & Zhu, 2018). Commensalism occurs when one partner benefits and the other partner is unimpacted. For example, during nitrification, *Nitrosomas* first oxidize ammonium to nitrite, then *Nitrobacter* oxidize nitrite into nitrate (Gee, Pfeffer & Suidan, 1990). *Nitrobacter winogradskyi* uses energy from the oxidation of nitrite to nitrate, meaning the presence of *Nitrosomas* benefits them, but *Nitrosomas* remain unaffected (Starkenburg et al., 2006). Lastly, parasitism is defined as one partner benefiting and the other being harmed. For example, malaria is caused by Plasmodium, which is transmitted to humans through the vector of mosquitos, causing severe illness (Sato, 2021). There are hundreds of other subcategories of symbiotic relationships, however, the term symbiosis also encompasses those where the effect of the symbiont on the host is unknown.

Researchers often focus on the associations between pathogenic microbes and organisms, with the view that bacterial infections are either harmful or irrelevant. However, throughout the last 20 years, there has been increased scientific focus on mutualistic symbiotic relationships (Moran, 2006).

Human Microbiome

Mammals, and in particular humans, represent some of the most diverse and complex microbial ecosystems, harboring 10-100 trillion bacteria (Qin et al., 2010). Studies into the human microbiome began with Antonie van Leeuwenhoek who in the 1680s compared his oral and fecal microbiota and noticed a distinct difference in the morphologies of the microbes present in both samples (Dobell, 1920). Antonie van Leeuwenhoek did this using a basic microscope he constructed himself (Leewenhoek, 1684). Nowadays, several microbiome projects have been launched worldwide in an attempt to understand the role of bacterial symbionts in the human body (Ursell et al., 2012). These include powerful molecular techniques and sequencing methods, culture-independent methods to characterize the microbiota, and a molecular phylogenetic approach to classify diversity (Qin et al., 2010).

Development of each individual human's microbiome, meaning the total DNA content of microbes inhabiting a human body (Ursell et al., 2012), begins at birth and develops dynamically. Microorganisms inhabit the skin, mouth, gut, vagina and most environmentally exposed surfaces (Round & Mazmanian, 2009). The largest proportion of bacteria resides in the gastrointestinal tract, acting as an essential component of human health (Ley, Peterson & Gordon, 2006). The symbiotic bacteria in the human gut have been shown to provide essential nutrients, metabolize compounds indigestible by humans, and defend against pathogenic bacteria (Dethlefsen, McFall-Ngai & Relman, 2007). Thus, the relationship between most microbes and humans is mutualistic, while few bacteria can colonize and demonstrate pathogenic characteristics.

Microbiomes vary significantly between individuals, irrespective of whether they are healthy or not, making it challenging to define a 'healthy microbiome'. The variation is due to various features including age, geography, lifestyle, and diet (Hollister, Gao & Versalovic, 2014). Dysbiosis, disruption in microbial homeostasis, has been associated with several diseases, including inflammatory bowel disease, multiple sclerosis, diabetes, allergies, autism, cancer, and asthma (Lloyd-Price, Abu-Ali & Huttenhower, 2016). Thereby, understanding more about the profound impact that the human microbiome has on health would greatly aid in preventing or improving disease onset. While there is a focus on in-depth research into the gut microbiota, the rest of the human body, including the oral cavity, is underexplored.

Human Oral Microbiome

The oral microbiome contains more than 700 species of bacteria, making it the second most diverse micro-environment on the human body, after the gut microbiome (Lu, Xuan & Wang, 2019). The diversity may be largely due to the various habitats it provides, including the teeth, gingival sulcus, tongue, cheeks, hard palate, soft palate, and tonsils (Arweiler & Netuschil, 2016). Moreover, the oral cavity is the gateway to numerous other sites in the human body, including the pharynx, esophagus, eustachian tube, trachea, lungs, nasal passages, and sinuses (Dewhirst et al., 2010). The microorganisms from the oral cavity often spread on adjacent epithelial surfaces or through saliva to the aforementioned neighboring sites (Dewhirst et al., 2010).

Approximately 280 bacterial species that reside in the oral cavity have been isolated in culture and named. Nonetheless, 16S rRNA gene-based sequencing studies identify around 700 species commonly present in human oral cavities (Deo & Deshmukh, 2019). The total 700 species found belong to 185 different genera and 12 phyla (Zhao et al., 2017). 54% are named, 14% are unnamed but cultivated, and 32% are uncultivated (Zhao et al., 2017). The phyla include Firmicutes, Fusobacteria, Proteobacteria, Actinobacteria, Bacteroidetes, Chlamydiae, Chloroflexi, Spirochetes, SR1, Syngleristes, nTM7 and GN01 (Perera et al., 2016).

Oral bacteria are vital for human health, as they function to contribute to host defenses, thereby preventing colonization of pathogens. For example, an oral cavity resident known as *Streptococcus salivarius* produces a bacteriocin that inhibits the adherence of pathogenic *Streptococcus pneumoniae*, resulting in reduced colonization of the mouth by the pathogen (Manning et al., 2016). This is the case for several bacteria that can change environmental conditions in the mouth to suppress opportunistic pathogens (Marsh, 2000). Nonetheless, interruption of the oral homeostasis may occur by pathogenic bacteria, leading to oral infectious diseases including tooth decay, periodontitis (gum disease), root canal infections, and tonsillitis (Kilian et al., 2016). Furthermore, there is upcoming evidence that oral bacteria may be linked to various systemic diseases such as cardiovascular disease, stroke, preterm birth, diabetes, arthritis, and pneumonia (Li et al., 2000; Han & Wang, 2013; de Pablo et al., 2009; Chapple & Genco, 2013).

Within the womb, the fetus is sterile, with the exception of occasional bacterial colonization through the amniotic fluid (Sampaio-Maia & Monteiro-Silva, 2014). During delivery, the baby encounters the microbiota of the uterus and the vagina of the mother, in addition to the atmosphere at birth. Babies birthed naturally often are colonized by vaginal bacteria, and babies born through C-section are usually first colonized by skin microbiota (Neu & Rushing, 2011). Despite the rapid colonization of newborn babies by bacteria, fungi, and other protists, the oral cavity typically remains sterile until the first feeding (Kennedy et al., 2019). The 'pioneer species', initial colonizers, of the oral cavity may comprise *Streptococcus*, *Lactobacillus*, *Actinomyces*, *Neisseria* and *Veillonella* (Deo & Deshmukh, 2019). Following the eruption of teeth, the microbiota can colonize non-shedding oral surfaces. For example, gingival crevices develop for periodontal microbes, and plaque accumulates where specific microbes thrive (Deo & Deshmukh, 2019). This developmental process allows for high-species diversity within the oral cavity. During old age teeth are often lost, and this results in a succession of flora similar to that before tooth eruption (Patil et al., 2013).

Adhesive Fimbriae

Bacteria use long proteinaceous appendages on their cell surface to interact with external environments, referred to as fimbriae or pili. They are non-flagellar thread-like structures that consist of covalently and non-covalently interacting repeated pilin subunits (Lukaszczuk, Pradhan & Remaut, 2019). While their primary role is to adhere to external environments, they can also be involved in host cell invasion, DNA and protein secretion uptake, biofilm formation, and cell motility (Pizarro-Cerdá & Cossart, 2006). There is a range of distinct pilus classes depending on their

structure, biogenesis, function and whether the bacteria are gram-positive or negative (Hospenthal, Costa & Waksman, 2017).

Fimbriae play an essential part in the interaction between the bacterial cells and host cells. They bind to various host proteins, assist in immunogenicity, stimulate cytokine production, and promote bone resorption (Hamada et al., 1998). Bacterial pathogens also utilize fimbriae to harm their hosts. For example, the fimbriae of *Prevotella intermedia* induce a hemagglutination reaction and those of *Prevotella loescheii* cause coaggregation with other bacteria (Hamada et al., 1998).

Bacteria within the mouth often form communities by adhering to oral surfaces and each other. Their relationships with other bacteria influence their ability to persist in their environment. Over time, the evolution of oral bacterial communities is influenced by features including selective adherence to either tooth surfaces or epithelium, cell to cell binding, and interaction between the different bacterial species within the mouth (Deo & Deshmukh, 2019). Different surfaces within the mouth are colonized predominantly by specific bacteria due to specific adhesins which bind to complementary receptors on the oral surface (Aas et al., 2005). Overall, the fimbriae of all bacteria, particularly oral cavity microbiota, are key components in interactions between the host and bacteria.

Multicellular Bacteria

Multicellular bacteria exist in a multitude of differing ecosystems, including the mouth. Multicellular bacteria can be defined by two factors, having cell-cell adhesion to form a new evolutionary unit, and having intercellular communication leading to coordinated activity (Lyons & Kolter, 2015). There are certain disadvantages that come with the formation of multicellular bacteria. This includes energetic costs building up from adhesion and communication, and physical limitations resulting from reduced movement possibilities (West et al., 2006). However, there is a range of advantages that come with multicellularity. Multicellular filaments are more resistant to physical and chemical stress, benefit in feeding abilities, are more protected from predation, colonize new environments more effectively, and have increased survival probability in conflicts with other microbes (Lyons & Kolter, 2015; Bonner, 1998; Kaiser, 2003). These benefits are primarily due to the physical adhesion of the cells to each other, creating a large unit. Multicellularity may result in bacteria within a filament either exhibiting different characteristics or being identical. Filamentous oral bacteria often have phenotypic differences despite being in the same genus (Rossetti et al., 2013). Overall, multicellular bacteria often display unique characteristics and intrinsically differ from model rod organisms.

Rod-shaped Bacterial Reproduction

Investigations into model organisms have given major insights into bacterial cell replication, not just into the growth of new cells but also DNA replication and division. Model organisms such as *E. coli* and *B. subtilis* are thoroughly investigated due to their fast growth rate and ability to adapt rapidly to diverse environments. Most importantly, they can survive without intricate associations with other species. While understanding these model organisms is vital, most microorganisms in their natural environments are likely to endure complex relationships with other species. The

reliability of microorganisms to each other and eukaryotes illuminates why 99% of microbes, particularly symbionts, are impossible to culture (Moran, 2006). Most symbiotic host partners, larger eukaryotic organisms, are unsuitable for genetics and development laboratory studies, making them challenging to study *in vivo* (Moran, 2006).

E. coli reproduction entails the replication of its DNA, the elongation of the cell and then constriction in the middle of the elongated cell so that two daughter cells form (Egan & Vollmer, 2013). The rod shape in *E. coli* and *B. subtilis* is maintained by the incorporation of peptidoglycan (PG) along the sidewalls, and during cell elongation, there is no evidence of new PG incorporation at the two poles (Mobley et al., 1984), but the new PG is built up along the sidewalls, facilitating lateral elongation. Namely, model rod-shaped organisms elongate first and then divide transversely, i.e., along their width axis. The two main complexes of growth and division are the elongasome, which inserts PG along the long axis of the rod during growth, and the divisome which facilitates constriction and new PG synthesis at the cell center (Typas et al., 2011). They are composed of scaffolding cytoskeletal-like proteins, inner membrane-spanning elements, and periplasmic enzymes (Egan & Vollmer, 2013).

Longitudinally Dividing Bacteria

While focusing on model organisms is important, extending observations into non-model organisms is vital to understand bacterial replication and growth. Most bacteria utilize transverse binary fission, but some bacteria have been reported to undergo longitudinal fission.

Three examples of non-model bacteria with differing cell division modes with respect to model bacteria are the ectosymbionts *Candidatus Thiosymbion oneisti* and *Candidatus Thiosymbion hypermnestrae*, and the endosymbiont *Spiroplasma poulsonii*. *Ca. T. oneisti* and *Ca. T. hypermnestrae* attach themselves by one pole to their host partners *Laxus oneisti* (Polz et al., 1994) and *Robbea hypermnestra* (Ott et al., 2014), respectively. *S. poulsonii* lives within the hemolymph of the fruit fly *Drosophila melanogaster* (Herren et al., 2014).

S. poulsonii was observed to assume 'Y-shapes' that eventually proved to be due to longitudinal scission (Ramond et al., 2016). Moreover, this shape was observed in *Spiroplasma citri*, signifying this may be a common occurrence in the *Spiroplasma* clade. This mode of division was hypothesized to be related to the motility of *Spiroplasma* (Shaevitz, Lee & Fletcher, 2005). *Spiroplasma* have long contractile fibers that run from one end of the cell to the other, and longitudinal division allows the preservation of the network of fibers to ensure they are not cut in half (Ramond et al., 2016).

In *Ca. T. oneisti*, through incubation with PG metabolic probes, Pende et al., 2018 observed that the insertion of a new cell wall began at the poles and proceeded inwards along with the FtsZ-based membrane constriction (Pende et al., 2018). The closest relatives of the symbionts are free-living sulfur oxidizers that live in anoxic conditions. *Ca. T. oneisti* has been hypothesized to have evolved from a free-living bacterium living in anoxic sand zones due to its propensity to oxidize sulfur, proliferate and downregulate stress-related genes in anoxia (Paredes et al., 2021).

The free-living bacterium may have evolved from a flagellated anaerobe with transverse cell division that then evolved into the symbiotic and longitudinally dividing *Ca. T. oneisti* (Paredes et al., 2021). The potential advantages acquired from this symbiotic relationship include the ability to consume nutritional compounds from the nematode, including phospholipids and organic carbon compounds, and protection from predators (Paredes, 2021). Furthermore, the symbiont may have eventually optimized mechanisms to resist oxidative stress and utilize metabolic pathways to exploit the oxygenated sand zones rather than the anoxic ones (Paredes et al., 2021). The array of advantages given from attachment to a host may have pushed the evolution of the reproductive mode to longitudinal (Paredes, 2021).

Bacterial Chromatin

DNA also needs to be replicated and segregated faithfully for complete bacterial reproduction. The length of a bacterial chromosome is significantly longer than the average cell length and thereby requires large-scale compaction to fit inside the cell (Reyes-Lamothe, Wang & Sherratt, 2008). For successful DNA segregation, the subcellular organization of the nucleoid, the compacted region containing all the genetic material, specifically DNA, RNA, and structuring proteins, is essential. When compacted, the nucleoid usually takes up 15-25% of the cell volume (Joyeux, 2015), is highly structured but dynamic, and undergoes several reorganization stages during the cell cycle and under differing physiological conditions (Kisner & Kuwada, 2020).

The forces imposing compaction include supercoiling, DNA-binding proteins, transcription, and molecular crowding (Shen & Landick, 2019). While there are a variety of intrinsic physical and chemical forces, this paragraph will focus on the extrinsic forces imposed by nucleoid-associated proteins (NAPs) (Krogh, Møller-Jensen & Kaleta, 2018). NAPs are highly conserved within bacteria and other prokaryotic species, suggesting an advantage of nucleoid structuring that improved the course of evolution (Krogh, Møller-Jensen & Kaleta, 2018). NAPs bind throughout the genome with variable degrees of specificity; however, many prefer AT-rich sites as these are intrinsically more unstable areas of the chromosome (Gordon et al., 2011). NAPs also have a variety of possible roles in DNA alteration, including bending DNA, wrapping around the DNA, bridging two distinct domains, and disrupting existing structures (Lioy et al., 2018; Macvanin & Adhya, 2012).

The most abundant and highly conserved NAP in growing bacteria is HU, which plays a role in nucleoid structure and gene transcription (Macvanin & Adhya, 2012). It is a ten kDa protein that binds to supercoiled areas of the DNA with no sequence specificity (Bonney & Rouvière-Yaniv, 1991). HU functions to bend DNA, wrap DNA, constrain supercoils, bridge DNA and facilitate the formation of RNA-DNA complexes (Qian, Zhurkin & Adhya, 2017; Hammel et al., 2016; Kobryn, Lavoie & Chaconas, 1999; Broyles & Pettijohn, 1986; van Noort et al., 2004). Another example of a NAP is histone-like nucleoid structuring protein (H-NS). H-NS binds to AT-rich regions of DNA and inhibits transcription (Lucchini et al., 2006). It inhibits gene expression through the formation of nucleoprotein filaments, either linear filaments where it binds to one area of DNA, or bridged filaments where it binds to two DNA areas (Liu et al., 2010). H-NS disruption occurs by elongation of RNA

polymerase where elongation complexes disrupt the filament covering a promoter, and H-NS silencing may be halted (Rangarajan & Schnetz, 2018).

Chromosome Configuration

DNA replication begins bi-directionally at a specific chromosome region that is referred to as the origin of replication (*ori*). The two replication forks meet at the region opposite the *ori*, referred to as the terminus (*ter*) region. The organization of the *ori* and *ter* regions in the chromosome have been described in two distinct spatial patterns in model organisms. One mode of organization is described as longitudinal in which the *ori* is at one pole and the *ter* at the other, also referred to as *ori-ter* configuration (Wang & Rudner, 2014). The other mode is referred to as transverse configuration, where the *ori* and *ter* are positioned at mid-cell where the left and right chromosome arms are present in separate cell halves, also referred to as left-*ori*-right arrangement (Wang & Rudner, 2014). These patterns were first described in *B. subtilis*, *C. crescentus* and *E. coli* (Lin, Levin & Grossman, 1997). Most bacteria, including *E. coli* and *B. subtilis*, also commonly alternate between the two chromosome configurations, depending on cell cycle stage and environmental conditions (Wang & Rudner, 2014).

Weber et al., 2019 discovered the chromosome configuration in longitudinally dividing *Ca. T. oneisti* is transverse, with the *ori* and *ter* being in the middle of the cell (Weber et al., 2019) (Figure 1). Strikingly, for a non-monoflagellated rod, and for a transverse chromosome configuration, the chromosome configuration is kept semi-constant, i.e. the location of the *ori* does not fluctuate depending on cell cycle stage but stays at the same position throughout generations. The *ter* migrates to the poles during the cell cycle but ends up at mid-cell after division has completed. We will henceforth refer to this chromosome configuration as “semi-fixed configuration” because it is maintained transgenerationally with the *ori* at mid-cell, and the *ter* moving dynamically throughout the cell. Additionally, the localization pattern of ParB was identical to that of the *ori*, and recombinant ParB bound to a *parS* site close to the *ori*, meaning the chromosome segregation is likely mediated by a ParABS system (Weber et al., 2019). The chromosome configuration was postulated to be an adaptation to symbiosis, as maintaining the intracellular localization of genes may facilitate the compartmentalization of the symbiont cell into a host and environment side (Weber et al., 2019).

This insight led to investigations into the chromosome configuration of *Ca. T. hypermnestrae*, another longitudinally dividing symbiont. The chromosome configuration in *Ca. T. hypermnestrae* was observed to be longitudinal, with the *ori* at the host attached site and the *ter* at the other pole (Viehboeck, Weber et al., manuscript in preparation) (Figure 1). Moreover, the chromosome configuration remained constant, i.e., *ori* and *ter* occupied the same subcellular region throughout the entire cell cycle. We will henceforth refer to this chromosome configuration as “fixed configuration”.

To determine the chromosome configuration of a non-nematode but mammalian symbiont, FISH on *A. filiformis* *ori* and *ter* regions was performed (Viehboeck, Weber et al., manuscript in preparation). The *ori* was found at the host-attached pole and the *ter* at the most distal pole, a longitudinal configuration (Figure 1). Similarly to the

nematode symbiont *Ca. T. hypermnestrae*, the chromosome configuration remained unchanged depending on the cell cycle stage. The chromosome configuration in *Ca. T. hypermnestrae* and *A. filiformis* can thereby be referred to as fixed chromosome configurations because the configuration remains unchanged throughout the cell cycle, as well as transgenerationally. These insights all pushed for further investigations into the chromosome configuration of symbiotic bacteria and how these differ from non-symbiotic bacteria.

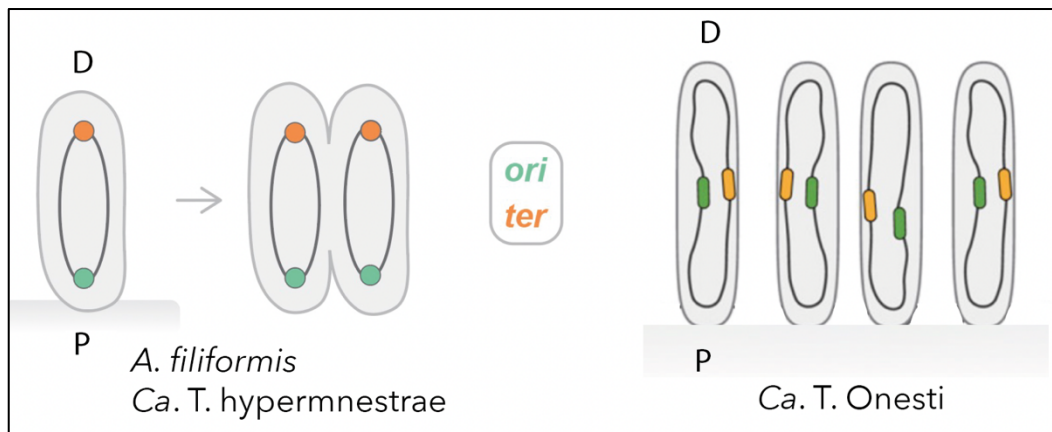


Figure 1. Chromosome configuration of *A. filiformis*, *Ca. T. hypermnestrae* and *Ca. T. oneisti*. The left drawing displays the longitudinal chromosome configuration observed in *A. filiformis* and *Ca. T. hypermnestrae* with the *ori* oriented towards the host proximal pole and the *ter* at the distal pole. The right drawing demonstrates the transverse chromosome configuration of *Ca. T. oneisti* with the *ori* and *ter* organized at mid-cell. D is distal, and P is proximal. *ori* is green, and *ter* is orange. (Figures adapted from Viehboeck, Weber et al., manuscript in preparation, and Weber et al., 2019).

***E. coli* Chromosome Segregation**

Chromosome replication and segregation are tightly controlled processes that ensure that DNA is replicated and at least one copy of the chromosome is present in the daughter cells (Reyes-Lamothe, Nicolas & Sherratt, 2012). *E. coli* has a 4.6-Mbp circular chromosome organized in a highly specific manner comprising the nucleoid (Niki & Hiraga, 1998). Most bacteria appear to have a single large circular chromosome, making them monoploid. However, it has recently become more evident that many prokaryotic species are polyploid, including many archaea and cyanobacteria (Soppa, 2021). Moreover, some species have multiple differing chromosomes, such as *Rhodobacter sphaeroides*, which has one chromosome that is 3.0-Mbp and a second one that is 0.9 mb (Mackenzie, Simmons & Kaplan, 1999) or *Burkholderia cepacia* which has three distinct chromosomes (Agnoli et al., 2012).

In *E. coli*, one proposed method of sister chromosome segregation is through a spontaneous de-mixing of chromosomes related to entropic forces during DNA replication within the cell (Gogou, Japaridze & Dekker, 2021). A homogenous mixture of two polymers was discovered to be entropically unfavorable when confined to a cylindrical cell volume, so following DNA replication, the two chromosomes spontaneously segregate to maximize entropy (Jun & Mulder, 2006).

The chromosome configuration of *E. coli* has been well studied. In newborn slow-growing *E. coli* cells, *ori* is localized at the old pole border and *ter* at the new pole border. As the DNA begins to replicate, one copy of replicated *ori* migrates to the opposite pole border, and the other *ori* copy remains at the old pole border (Niki & Hiraga, 1998). Meanwhile, the *ter* segment migrates from the pole to mid-cell and is retained there until the terminus is duplicated (Niki & Hiraga, 1998) (Figure 2). The *ori* and *ter* regions of the chromosome move dynamically around the cell, playing a critical role in the successful chromosome replication, partitioning and cell division of *E. coli*. The *ori* and *ter* locations have also been observed to differ depending on environmental conditions, namely whether fast or slow growth is occurring (Niki & Hiraga, 1998).

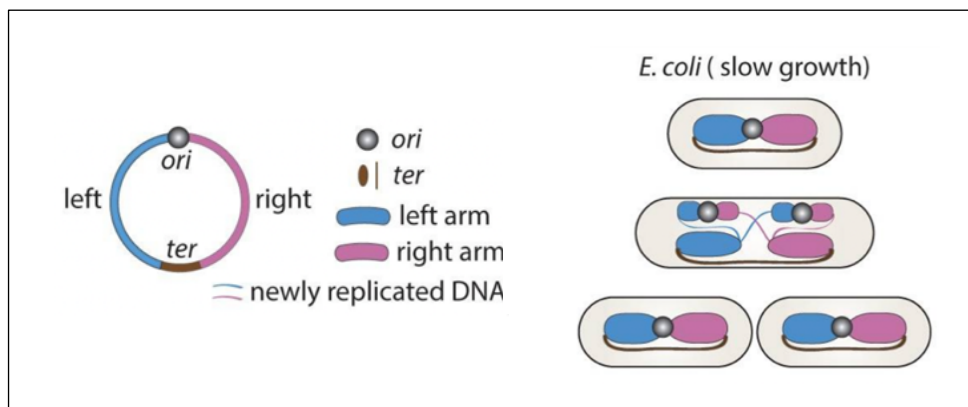


Figure 2. *E. coli* chromosome segregation. Left demonstrates the *E. coli* chromosome, more specifically the *ori*, *ter* and two arms of the chromosome. Right demonstrates the process of chromosome segregation of *E. coli* during slow growth. The chromosome starts in transverse configuration, and the *ori* moves around the cell during segregation until the cell is divided and transverse configuration is resumed. Grey is *ori*, brown is *ter*, blue is left arm of the chromosome, and pink is right arm of the chromosome. (Figure from Niki & Hiraga, 1998).

ParABS-Mediated Chromosome Segregation

While *E. coli* undergoes the aforementioned chromosome segregation and organization method, numerous bacteria undergo a ParABS mediated chromosome segregation mechanism. The *par* locus was first discovered in low-copy number plasmids and was demonstrated to be essential for their stable inheritance (Abeles, Friedman & Austin, 1985; Mori et al., 1986). The ParABS system may be conserved in up to two-thirds of bacterial species (Toro et al., 2008). The system has been found in *Myxococcus xanthus*, *Caulobacter crescentus*, and *Vibrio Cholerae*. It is essential in a variety of bacteria; for example, without ParA and ParB, *M. xanthus* and *C. crescentus* do not replicate viably (Iniesta, 2014; Mohl, Easter & Gober, 2008).

The ParABS system is made of ParA, an ATPase protein, ParB, a CTPase and DNA-binding protein and *parS*, a centromere-like DNA site. *parS* sites are commonly located near the *ori* and are the first DNA locus of the three to be segregated after chromosome replication (Livny, Yamaichi & Waldor, 2007). ParB binds to and nucleates on *parS* sites and recruits additional ParB molecules to non-specific DNA

to form a network of protein-DNA complexes (Funnell, 2016). ParB also recruits the structural maintenance of chromosome (SMC) complex to the chromosome to reduce DNA entanglement and promote the individualization of replicated chromosomes (Minnen et al., 2011). These complexes stimulate the ATPase activity of ParA, creating a ParA-ATP gradient (Hwang et al., 2013). The chromosome's origin-proximal region is subsequently driven along the gradient to the opposite side of the cell pole, finalizing chromosome segregation (Vecchiarelli, Neuman & Mizuuchi, 2014). The ParABS and SMC coordinate chromosome segregation and chromosome organization together in many bacterial species.

A. filiformis*, *S. muelleri*, *C. steedae

The focus of this study will be three oral cavity symbionts called *A. filiformis*, *S. muelleri* and *C. steedae*. They are Gammaproteobacteria that belong to the family *Neisseriaceae* (Hedlund & Kuhn, 2006). All three are aerobic, gram-negative, chemoorganotrophic bacteria that have a unique morphology (Hedlund & Kuhn, 2006). They form distinguished multicellular filaments making them easily discernible from each other and other bacterial species. Up to now, the three bacteria have been found exclusively in the oral cavities of warm-blooded vertebrates, including sheep, dogs, humans, and chickens (Steed, 1962; Nyby et al., 1977). While they have been discovered to be on the tongue, throat, gingival margin and more, they are most abundantly found attached to the hard palate of the mouth (Hedlund & Kuhn, 2006). Data from the human genome project showed that 35% of humans have *S. muelleri*, and 45% of humans have *A. filiformis* (T. Viehboeck, unpublished).

A. filiformis form ribbon-like filaments composed of disk-shaped cells that attach by one pole to the host surface (Figure 3), similarly to the longitudinally dividing symbionts *Ca. T. oneisti* and *Ca. T. hypermnestrae* (Tønjum, 2015). *S. muelleri* form shorter filaments composed of crescent-shaped cells that attach through two poles to the host surface (Figure 3) (Hedlund & Tønjum, 2015). *C. steedae* are also crescent-shaped cells, albeit larger than *S. muelleri*, that attach by two poles to the host surface (Figure 3). They inhabit the mouth by adhering to the mucosal squamous epithelium that composes the hard palate with their fimbriae (Hedlund, 2002). They colonize the oral cavity through their ability to glide and adhere to new epithelial cells despite the constant desquamation of the epithelial cells and their removal in saliva.

In the 1960's it was shown that *S. muelleri* and *A. filiformis* have fimbriae through TEM images on which fine fibroid structures were visible - the fimbriae (Pangborn, Kuhn & Woods, 1977; Kaiser & Starzyk, 1973). Interestingly, both the *S. muelleri* and *A. filiformis* fimbriae localized to one area of the cells. In *A. filiformis* the fimbriae were detected on the proximal pole of the cell and in *S. muelleri* the fimbriae were detected on the host-proximal side. The host-proximal side of *S. muelleri* was previously referred to as the ventral or concave side, and the opposite side was referred to as the dorsal side. The dorsal side of the cell did not have any fimbriae present, signifying the fimbriae are ventrally polarized. Up to this point, polarization of fimbriae on *C. steedae* has not been identified.

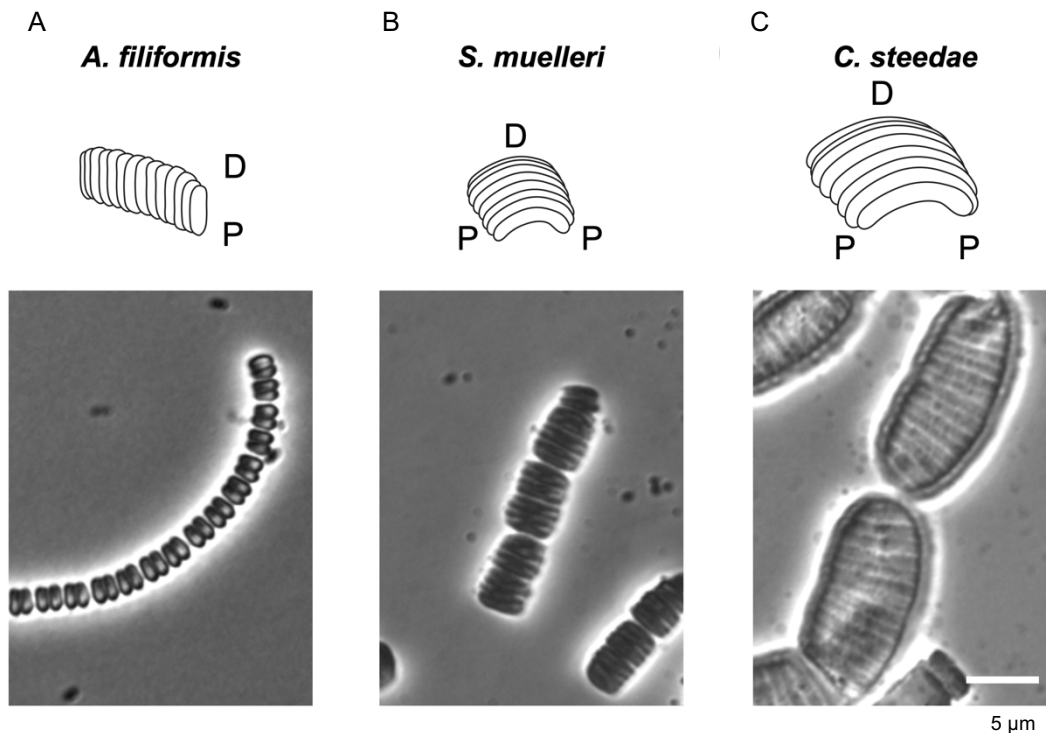


Figure 3. Phase-contrast microscopy images of *A. filiformis*, *S. muelleri* and *C. steedae*. (A) The upper panel is a diagram representing the rod shape of *A. filiformis*, and the lower panel is a phase-contrast microscopy image of *A. filiformis*. (B) The upper panel is a diagram representing the crescent shape of *S. muelleri*, and the lower panel is a phase-contrast microscopy image of a top view of *S. muelleri*. (C) The upper panel is a diagram representing the crescent shape of *C. steedae*, and the lower panel is a phase-contrast microscopy image of a top view of a *C. steedae* filament with its proximal (ventral) side facing up. Scale bar 5 μm . D is distal, and P is proximal (Figure from Nyongesa, Weber et al., under revision at Nature Communications).

At the present time, the role that these three bacteria play in the oral cavity is unknown. However, a closed genome for the three bacteria is available, giving some insight into their possible roles. The genomes are all approximately 2.4 Mbp in size and have a GC content of 46% (*A. filiformis*), and 41% (*S. muelleri*), and 50.5% (*C. steedae*). *A. filiformis* and *S. muelleri* contain no plasmids, but *C. steedae* contains two plasmids. One plasmid is 25 kB and present in multiple copies within the cell, and the second plasmid is 80 kB, with lower copy numbers than the small plasmid (T. Viehboeck, unpublished data). Their genomes encode for TonB-dependent vitamin B₁₂ transporter and vitamin B₁ transporter (T. Viehboeck, unpublished data). Additionally, they encode for amino acid transporters and free iron. Furthermore, they have been found to contain host lysozyme inhibition proteins such as PliC, and have resistance to host neutrophils (T. Viehboeck, unpublished data). Antibiotics have also been found to be encoded in their genomes and secretion systems to mediate the secretion of proteins, playing a possible role in host-symbiont interaction. Lastly, they possess genes possibly encoding similar cytokinetic machinery of *E. coli* (T. Viehboeck, unpublished data). The genomes suggest they can take up and exploit organic compounds and nutrients found in saliva and may tolerate the host immune system and produce antibiotic effectors to deter pathogens.

Aim

Investigations into the chromosome biology of two nematode-attached symbionts revealed that they are vertically polarized, their chromosome configuration is fixed or semi-fixed, and their segregation is likely mediated by the ParABS system. *A. filiformis* was also observed to be vertically polarized with a longitudinal chromosome configuration, but, up to this thesis, there was a gap in knowledge surrounding the chromosome biology of *S. muelleri* and *C. steedae*, which also belong to the *Neisseriaceae* family. This study aimed to determine the chromosome configuration of both *S. muelleri* and *C. steedae*, observe if they display a fixed configuration and, more generally, whether this cell biological feature is an adaptation to the symbiotic lifestyle.

Firstly, I developed a qPCR method to quantify oral cavity symbiont cells. This is highly advantageous for producing reliable and reproducible results in future experiments. Additionally, the qPCR primers produced from the study may be used in the future to test human samples for the presence of *Neisseriaceae*, specifically the genera *Alysiella*, *Simonsiella* and *Conchiformibius*.

Secondly, I performed a western blot and subsequently an immunostaining with an anti-fimbriae antibody to find out whether *C. steedae* fimbriae localization is polar. Whereas *A. filiformis* and *S. muelleri* have previously been reported to have fimbriae that are polarly localized, the fimbriae localization had not been analyzed thus far in *C. steedae*.

Lastly, I determined the chromosome configuration of *S. muelleri* and *C. steedae* using DNA-FISH-based localization of *ori* and *ter* in both bacteria, as well as the localization of the large plasmid in *C. steedae*.

Overall, this study aims to make advances in understanding chromosome biology of non-model organisms such as oral cavity symbionts belonging to the *Neisseriaceae* family.

Methods

***A. filiformis*, *S. muelleri* and *C. steedae* strains and cultivation**

A. filiformis, *S. muelleri* and *C. steedae* were ordered from the “Leibniz Institute DSMZ-German Collection of Microorganisms and Cell Cultures” (DSM No.: 16848, DSM No.: 2579, DSM No.: 2580). For all experiments, the bacteria were prepared as described below.

A. filiformis

50 µl of a stock of *A. filiformis* frozen at -70°C stored in 15% glycerol was inoculated into a baffled flask containing 50 ml of PY medium (Table 1) and grown overnight in a shaking incubator at 120 rpm at 37°C. After 16 hours, 100 µl of these cultures were transferred to an Erlenmeyer flask containing 100 ml of modified PY medium (Table 2).

S. muelleri

50 µl of a stock of *S. muelleri* frozen at -70°C stored in 15% glycerol was placed onto a BSTSY agar plate (Table 3), spread on the plate, and the plate was placed in a 37°C incubator. After 24 hours of growth, colonies were inoculated from the plate into an Erlenmeyer flask containing 100 ml of meat extract medium (Table 5) or BSTSY medium (Table 4) and grown overnight in a shaking incubator at 120 rpm at 37°C.

C. steedae

50 µl of a stock of *C. steedae* frozen at -70°C stored in 15% glycerol was placed onto a BSTSY agar plate (Table 3), spread on the plate, and the plate was placed in a 37°C incubator. After 24 hours of growth, colonies were inoculated from the plate into an Erlenmeyer flask containing 100 ml of BSTSY medium (Table 4) and grown overnight in a shaking incubator at 120 rpm at 37°C.

Table 1- PY medium

Ingredient	Percentage
Peptone from meat	1.5% wt/vol
Yeast extract	0.3% wt/vol
NaCl	0.5% wt/vol
K ₂ HPO ₄	0.25% wt/vol

Table 2- Modified PY medium

Ingredient	Percentage
Peptone from meat	1.5% wt/vol
Yeast extract	0.3% wt/vol
NaCl	0.5% wt/vol
K ₂ HPO ₄	0.1% wt/vol

Table 3- BSTSY agar

Ingredient	Percentage
Tryptone soja bouillon without dextrose	2.75% wt/vol
Agar	1.5% wt/vol
Fetal bovine serum	10% wt/vol

Table 4- BSTSY medium

Ingredient	Percentage
Tryptone soja bouillon without dextrose	2.75% wt/vol
Fetal bovine serum	10% wt/vol

Table 5- Meat extract medium

Ingredient	Percentage
Meat extract	1.7% wt/vol
Yeast extract	0.7% wt/vol
NaCl	0.5% wt/vol

qPCR

Sample collection

After starting the growth of *A. filiformis* culture in modified PY medium, at hours 0, 2, 4, 6, 7, 8, 9, 10, 11, 12, 13 and 25, the optical densities at a wavelength of 600 (OD₆₀₀) of triplicate flasks were measured with a spectrophotometer and 1 ml samples were extracted. The 1 ml samples were centrifuged for 5 minutes at 16,000xg at 4°C and the supernatant was discarded. The samples were stored frozen at -20°C.

DNA extraction

A phenol-chloroform based DNA extraction was performed on the 1 ml samples that were taken from the *A. filiformis* flasks. The frozen samples were thawed on ice for 5 minutes, then each pellet was resuspended with TLB. The TLB was composed of 5M NaCl (100 mM final concentration), 1M Tris-HCl at pH 8.0 (10 mM f.c.), 0.5M EDTA at pH 8.0 (25 mM f.c.), 20% SDS (f.c. 0.5% v/v), and 0.1%-diethyl pyrocarbonate (DEPC)-treated water (final volume 1ml).

10 mg/ml RNase A (f.c. 2 mg/ml) was added to remove RNA from the sample. Lysozyme buffer was added to lysozyme to make 100 mg/ml (f.c. 2 mg/ml). Following heavy vortexing, the samples were incubated at 37°C 350 rpm for 30 minutes. 20 mg/ml of Proteinase K (f.c. 1 mg/ml) was added and vortexed. It was incubated at 50°C at 350 rpm for 30 minutes.

500 µl of phenol:chloroform:isoamyl alcohol (25:24:1, 1X volume) was added to the tube. It was vortexed for 1 minute and then centrifuged at maximum speed for 5 minutes at 4°C. The upper phase was transferred to a new 1.5 ml Eppendorf tube. 500 µl of chloroform:isoamyl alcohol (24:1, 1X volume) was added to the tube with the upper phase. It was vortexed for 1 minute again and centrifuged at maximum speed for 5 minutes at 4°C. The upper phase was again transferred into a new 1.5 ml Eppendorf tube.

7.5M of NH₄OAc (f.c. 2.5M) was added to the tube with the second upper phase extraction. 5 mg/ml of glycogen (5 µg) was added and mixed by vortexing. 2X of the current volume of 100% EtOH was added and again mixed with vortexing. The samples were incubated for 30 minutes at -20°C and then centrifuged for 30 minutes at maximum speed at 4°C, resulting in the formation of a pellet. The supernatant was carefully decanted, and the pellet was washed with 300 µl of 80% EtOH. It was vortexed and centrifuged for 15 minutes at 4°C at maximum speed. The supernatant was carefully pipetted off. The tube was quick spun to remove residual EtOH and left to air dry for 5 minutes. 30 µl of DEPC-H₂O was added, and it was set to shake for 1

hour at 37°C at 300 rpm in an incubator. Following vortexing and spinning down, the sample DNA concentration was measured with a Nanodrop and stored at -20°C.

Primer design

The primers used were designed using the primer3plus application (<https://www.bioinformatics.nl/cgi-bin/primer3plus/primer3plus.cgi>) and were produced by Microsynth (<https://www.microsynth.ch/home-ch.html>) (Table 6).

Table 6- Primers used for targeting *A. filiformis gyrB* and *rpoB* genes

<i>gyrB</i> amplicon length- 196 bp	Forward	GATGGCATGACCGTAGAATG
	Reverse	GCCTGATGTGTCAATTTTGG
<i>rpoB</i> amplicon length- 196 bp	Forward	ACAGCTTGGTAACGCAACAG
	Reverse	CAATTTTGTGTTTCGCCTTTG

PCR

To amplify the targeted DNA sequence, *gyrB* and *rpoB*, a PCR was carried out on a sample of *A. filiformis* extracted after 8 hours of growth. Master mix was made containing 10 mM forward primer (f.c. 0.2 mM), 10 mM reverse primer (f.c. 0.2 mM), 10 mM dNTPs (f.c. 0.2 mM), 1.25 U of Taq polymerase (f.c. 0.025 U), 25 mM MgCl₂ (f.c. 1.5 mM), 2X buffer (f.c. 1X) and H₂O (final volume 24 µl). 24 µl of the master mix was put into each PCR tube, and 1 µl of the template was added to 3 PCR tubes and 1 µl of DEPC-H₂O to the negative control.

Hot start PCR was run according to the cycle in Table 7.

Table 7- PCR cycle run

1x	30x			1X
95°C for 5 minutes	95°C for 30 seconds	55°C for 30 seconds	72°C for 30 seconds	72°C for 5 minutes

Following PCR, the samples were loaded onto a 1% agarose gel along with a 100 bp ladder, and the samples underwent gel electrophoresis. This allowed the detection of bands to observe whether they were at the expected heights corresponding to the length in between the forward and reverse primers. The PCR products were purified using the NEB Monarch® PCR and DNA Cleanup Kit (NEB, T1030) and sent to eurofins genomics for sequencing to confirm that the targeted DNA sequence was amplified.

Cloning and transformation of the DNA sequence

The cloning kit used was the pGEM®-T Easy Vector Systems Kit (Promega, A1360), which allows for distinction between bacteria that have taken up by the plasmid or not with blue-white screening. The ligation reaction was carried out by mixing 2X ligation buffer (f.c. 1X), 50 ng/µl pGEM-T easy vector (5 ng), 3 units/µl T4 DNA ligase

(f.c. 0.3 U/μl), 0.1%-DEPC-treated water (final volume 10 μl) and 15 ng/μl of purified PCR product. A positive control was also made in which 4 ng of DNA control (0.8 ng) was utilized instead of the PCR product.

Following the ligation reaction, the products were immediately transformed. Chemically competent top 10 *E. coli* cells were thawed on ice for 20-30 minutes. 1 μl of ligated sample and 10 μl of top 10 *E. coli* were added to a 1.5 ml Eppendorf tube. The mixture was kept on ice for 15 minutes. Then the mixture underwent heat shock for 45 seconds at 42°C. Subsequently, the mixture was quickly moved to ice for 5 minutes. 200 μl of SOC ultra-rich medium was added to the mixture, and it was incubated at 37°C for 1 hour at 150 rpm.

LB plates with the addition of 100 mg/ml ampicillin (f.c. 100 μg/ml), 100 mM IPTG (f.c. 1 mM) and 20 mg/ml X-gal were used to grow the transformed *E. coli*. The pGEM T-easy vector encodes for ampicillin resistance, and the multiple cloning region is within the LacZ coding region. Therefore, if the plasmid took up the insert, LacZ would not be produced however, if it did not, then the LacZ would be produced. The addition of IPTG and X gal allows the distinction between LacZ production when the colonies appear blue and no LacZ production when the colonies appear white.

100 μl of the ligated solution was put onto a plate and spread. The plates were kept overnight at 37°C. The vectors that were successfully transformed appeared as white colonies on the plate, and the unsuccessful ones as blue colonies.

Colony PCR

A master mix was made containing 10 mM forward primer (f.c. 0.2 mM), 10 mM reverse primer (f.c. 0.2 mM), 10 mM dNTPs (f.c. 0.2 mM), 1.25 U of Polymerase (f.c. 0.025 U), 25 mM MgCl₂ (f.c. 1.5 mM), 2X buffer (f.c. 1X) and DEPC- H₂O. 25 μl of the master mix was put into each PCR tube. A master plate was prepared in which the LB plate was split into several grids that were each numbered. With a pipette tip, a white colony was scraped off, and the tip was put into the PCR tube for approximately 1 minute. After 1 minute the tip was taken out and grazed onto 1 grid on the master plate. A total of 5 white colonies were scraped off per gene, each plated on a different grid number. 2 colonies from the positive control plate and 1 negative control without a colony also underwent PCR. The PCR tubes were centrifuged, and the PCR was run (Table 4).

A 1% agarose gel was made, and the PCR product run with a 1 kB plus ladder. The PCR products with the bands with corresponding sizes to the vector were then purified with NEB Monarch® PCR and DNA Cleanup Kit (NEB, T1030) and again sent to eurofins genomics to be sequenced.

Plasmid production and extraction

The results from the sequencing allowed for the identification of the colonies that have the inserted vector. From the master plate, the corresponding grid number was identified, and one colony in the correct grid was picked and put into 10 ml LB agar with ampicillin. This was left shaking at 37°C overnight to allow the *E. coli* to grow.

After 18 hours, the *E. coli* was centrifuged at 4°C for 15 minutes at full speed. Extraction of the plasmids was then performed using the PureYield™ Plasmid Miniprep System (Promega, A1223).

Linearization of plasmid

To use the plasmid as a qPCR standard, the plasmid must be linearized with a restriction enzyme to ensure equal access of the primers to the DNA strand. The restriction enzyme chosen must not be able to cut within the insertion site of the plasmid or cut the genes that were inserted. The buffer used was CutSmart universal buffer. In a 1.5 ml Eppendorf tube 10X buffer (1X f.c.), 10 units PstI-HF restriction enzyme (f.c. 1 unit), 1 ng DNA and DEPC-H₂O (final volume 20 µl) were mixed. It was incubated for 2 hours at 37°C.

Following the linearization of the plasmid, it was run on a 0.8% agarose gel to measure the corresponding band size. The band at the correct length was cut out and purified using the NEB Monarch® DNA Gel Extraction Kit. The amount of DNA was measured with a nanodrop, and it was sent to eurofins genomics for sequencing to confirm that the correct gene will be used as the qPCR standard.

qPCR

The standards were produced by making serial dilutions of the cut plasmid. The first standard was a 1:10 dilution of the linearized plasmid with DEPC-H₂O (final volume 10 µl), and then using that dilution standard 2 was made with another 1:10 dilution (final volume 20 µl) and so on. The range of standards was from approximately 10⁸-10¹ copies.

The samples also all underwent a 1:4 dilution with DEPC-H₂O (final volume 8 µl).

A master mix with 2X Luna Universal qPCR Master Mix (f.c. 1X), 10 mM forward primer (f.c. 0.25 mM), 10mM reverse primer (0.25 mM) and DEPC- H₂O was made, and 19 µl of the master mix was put into each qPCR tube, along with 1 µl of either the standard, the sample or H₂O for the negative control.

Each standard and sample were done in duplicates, and each time point consisted of triplicates so there were 6 total samples per time point.

The qPCR conditions were run according to Table 8.

Table 8- qPCR cycle run

1x	45x		1X
95°C for 2minutes	95°C for 15 seconds	60°C for 1 minute	55°C to 95°C in increments of 0.5°C every 5 seconds

Morphometric measurements

Phase-contrast images from the FISH experiments were used for the morphometric measurements of all three bacteria. The cells of *A. filiformis*, *S. muelleri* and *C. steedae* were dried on slides and treated with lysozyme for 1 hour at 37°C. *A. filiformis* was quantified using the Fil-tracer tool that comes with the ObjectJ installation on ImageJ (Nyongesa, Weber et al., under revision at Nature Communications). For *A. filiformis*, Fil-tracer measured the filament length, cell length and produced cell boxes equivalent to the width of the cell, thus, a high number of cells could automatically be measured. For *S. muelleri* and *C. steedae*, the filament length, cell length and cell boxes were added manually. After the cell boxes were made, each cell was checked manually to ensure that the length and width markers were in the appropriate areas.

Western Blotting

The bacteria were grown to an OD₆₀₀ of 0.5 and the culture was diluted 1:10 with DEPC-H₂O. 10 µl of bacterial dilution was placed into an Eppendorf with 6X loading dye sample buffer (f.c. 2X). It was boiled for 5 minutes at 99°C in a heat block and then spun down for 10 minutes at 10,000xg. The supernatant was removed carefully and transferred to a new tube.

NuPAGE Bis-Tris-Gel-4-12% 10 well pre-cast gels (Thermo Fischer Invitrogen, NP0321BOX) were utilized. The gel was placed into the chamber along with a dummy gel on the opposite side and both were locked in. Running buffer (MOPS SDS) was poured into the gel chamber and 10-20 µl of protein extracts were placed in each well. It was run for 1 hour at 200V and then removed carefully before the gel was transferred into water.

Following the gel chamber run, the blotting membrane was placed in water for 10 minutes and in 1X transfer buffer for 10 minutes. The gel was blotted onto Hybond ECL nitrocellulose membranes (Amersham Biosciences) by placing it against the membrane and running it in a chamber with transfer buffer for 1 hour at 100V. Subsequently, the membrane was inoculated in Ponceau S solution for 2-5 minutes and washed shortly in water. The membrane was cut into pieces, depending on which antibody had to be added to each section, and each cut section was washed in 1X PBS before incubation for 45 minutes in 5% milk with 1X PBS on a shaker. Each piece, except the negative control, was incubated in either a 1:1000 dilution of sheep polyclonal anti-*E. coli* K88 fimbrial protein AB/FaeG antibody (ab35292, Abcam) or anti- *C. crescentus* FtsZ antibody (kindly gifted by the Brun Lab). The antibodies were diluted in 5% milk with 1X PBS overnight with soft agitation at 4°C.

The primary antibodies were washed off with 5 washing steps for 6 minutes each in 5% milk and PBS under agitation. The second antibody (horseradish peroxidase-conjugated anti-sheep secondary antibody 1:10,000 (Amersham Biosciences) for the anti-fimbriae antibody and horseradish peroxidase-conjugated anti-rabbit secondary antibody 1:10,000 (Amersham Biosciences) for the anti-FtsZ antibody) was diluted in 5% milk, and 1X PBS solution and the membrane pieces were incubated for 1 hour at room temperature and shaking. The membrane pieces were washed 5 times for 6

minutes in 1X PBS and milk. The final wash was done for 10 minutes in 1X PBS with 0.1% tween 20. The protein-antibody complexes were visualized using ECL plus detection reagents (Amersham Biosciences).

Immunostaining

The bacteria were grown to an OD₆₀₀ of 0.155 for *S. muelleri* and 0.879 for *C. steedae*. For the anti-fimbrial immunostaining, fixation for 1 hour in 3% paraformaldehyde (PFA) and no lysozyme was used. However, differing fixation methods were tested to find the optimal one for anti-FtsZ immunostaining (Table 9). Fixation in PFA, methanol and ethanol were all tested in different combinations with and without lysozyme. Additionally, the samples were either in a tube during fixation or dried down on a slide following fixation. Following tube fixation, the cells were centrifuged for 2 minutes at 7000xg at room temperature and washed twice with PBS. Then they were resuspended in PBS with 0.1% tween 20 and washed one more time. Blocking was done for 1 hour in PBT with 2% bovine serum albumin (blocking solution) at room temperature. Cells were incubated with a 1:500 dilution of sheep polyclonal anti-*E. coli* K88 fimbrial protein AB/FaeG antibody (ab35292, Abcam) or a 1:500 dilution of rabbit polyclonal anti-*C. crescentus* FtsZ antibody (kindly gifted by the Brun lab) overnight at 4°C in blocking solution.

The following day the samples were washed three times in PBT then incubated with a 1:500 dilution of Alexa 555 conjugated anti-sheep antibody (Thermo Fischer Scientific) or Alexa 647 anti-rabbit antibody (Thermo Fischer Scientific) in blocking solution for 1 hour at room temperature. Unbound secondary antibody was removed with two washing steps, one in PBT and one in PBS. The cell pellets were resuspended in PBS with 5 ug/ml Hoechst for 20 minutes in the dark and then washed once and resuspended in PBS. Agarose slides were prepared by placing 35 µl of warm agarose on each slide, then placing a silan slide on top and letting it dry for 1 minute. The silan slide was removed leaving an agarose bed on which 1 µl of the sample was placed along with 0.75 µl of vecta shield. A cover slide was placed on top and then it was ready for microscopy.

Table 9- Immunostaining conditions

Immunostaining		
Fixation	Lysozyme	Location
1 hour 3% paraformaldehyde	No lysozyme	Slide and tube
	5 minutes lysozyme	Slide and tube
	10 minutes lysozyme	Slide and tube
	15 minutes lysozyme	Tube
1 hour 100% Methanol	No lysozyme	Slide
20 minutes 80% Ethanol	No lysozyme	Slide and tube
	10 minutes lysozyme	Slide

Fluorescence in-situ hybridization

Gene probes

For FISH, fluorescently labelled probes needed to be synthesized to bind to specific DNA areas. Probes were designed, synthesized by PCR and labelled with fluorophores at the predicted origin and terminus sites of *S. muelleri* and *C. steedae*, along with a DNA area on the *C. steedae* big plasmid. The origin and terminus sites were predicted using the Genskw application (<https://genskw.csb.univie.ac.at/>), which detects sequences that may represent the origin of replication, opposite of which the terminus should lie. Genskw calculates the incremental and cumulative skew of two selectable nucleotides for a given sequence using the formula $\text{Skew} = (\text{nucleotide1} - \text{nucleotide2}) / (\text{nucleotide1} + \text{nucleotide2})$. The global minimum of the GC-skew correlates with the origin of replication DNA sequence, and the global maximum correlates with the terminus location in prokaryotic genomes. Additionally, the maximum sequencing coverage correlates with the Genskw predicted origin and terminus (Figure 4). Additionally, several sequences known to be found close to the origin of replication, including *parS* motifs, were found close to this site. Sequence motifs such as the *dif* site was also confirmed to be close to the predicted terminus.

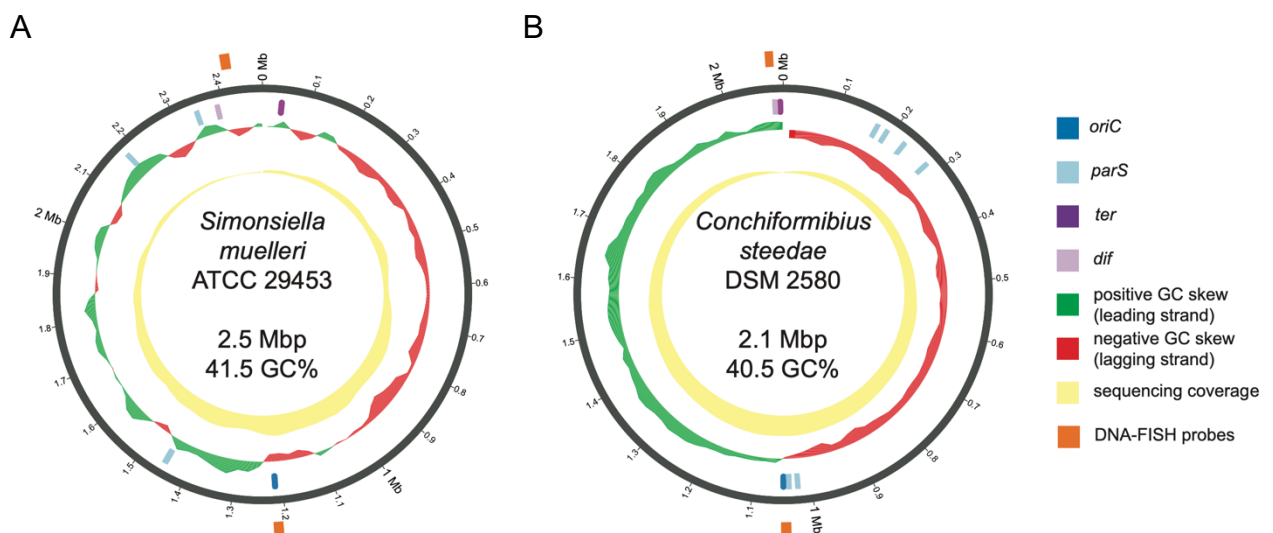


Figure 4. *S. muelleri* and *C. steedae* chromosome maps. (A) The circular map of *S. muelleri* genome (ATCC 29453) and (B) The circular map of the genome of *C. steedae* (DSM 2580). The black outer circle is the position in megabases of the genome. The middle circle represents the GC skew, green is positive, and red is negative. The yellow inner circle represents the sequencing coverage. *oriC* is dark blue, *parS* sequences are light blue, *ter* is dark purple, *dif*-sites are light purple, and the DNA-FISH probes are orange (Figure from Viehboeck, Weber et al., manuscript in preparation).

The set of polynucleotides were designed with the use of the Gene-Prober software (Moraru, C., 2021). 25 kB long fragments engulfing the origin and terminus were input into the software and several probes were designed for the origin sequence and terminus sequences. Of these, the 10 probes with the least distance between them were chosen for the origin sequence and 9 probes for the terminus sequence of *S. muelleri*, and 11 probes for the origin and 10 probes for the terminus of *C.*

steedae. The full sequence of the 80 kB *C. steedae* plasmid was input into Gene-Prober, and the 9 closest designed probes were selected. Each probe varied from 300-310 bp in length and varied in distance from 13-1300 bp between probes (Table 10).

Table 10- Polynucleotides used for FISH probes

Target	Probe No.	Primer	Sequence (5'-3')	Product (nt)
<i>S. muelleri</i> ori region (8,158 nt)	1	Sm_ori_1F	CAATGTAGATGCCGCTGAA	300
		Sm_ori_1R	CAACGATAGGTCACATTTGC	
	2	Sm_ori_2F	GATTTAGCAGCAGAACAACC	300
		Sm_ori_2R	GCCACAAATATCCACTACGT	
	3	Sm_ori_3F	CTATATATTCATTCGCTGGACG	300
		Sm_ori_3R	TTACCGCTTTTACGTGGG	
	4	Sm_ori_4F	ATTGATTACGTTGGCTCATG	300
		Sm_ori_4R	TTTTACGAGCAAGCTGTCT	
	5	Sm_ori_5F	GTGCTGATTTACGACGAAG	300
		Sm_ori_5R	CACCAATTGAGAAGTACGC	
	6	Sm_ori_6F	CCAAACCCACTACACATAAT	300
		Sm_ori_6R	GTTTTGGTGATCCTGAAAC	
	7	Sm_ori_7F	CAAATTAGCCAGCGGAATC	300
		Sm_ori_7R	TTTTGGGGCAGATTGATTC	
	8	Sm_ori_8F	TATTACCTAACTTTGCTCCG	300
		Sm_ori_8R	AAAAAGGAGTGTGTACCGA	
	9	Sm_ori_9F	TACTATCCTGCATAC CTGCA	325
		Sm_ori_9R	AATTTGGTGGCTACGAATG	
	10	Sm_ori_10F	CATTTGTGCAGTTTGGTTAG	300
		Sm_ori_10R	GTGAAAATGTCCATGAATCC	
<i>S. muelleri</i> ter region (8,187 nt)	1	Sm_ter_1F	GATTTGCGGTCAATCGTT	300
		Sm_ter_1R	GGGCAAATTC AATTCAGACC	
	2	Sm_ter_2F	ATGAAACCATCTGAACCGT	300
		Sm_ter_2R	CATTGATGCACTGGTTATTG	
	3	Sm_ter_3F	GATGATTTACGGATTTTAGCC	300
		Sm_ter_3R	CGTTCTCAATTTGTAGACCAAG	
	4	Sm_ter_4F	TCGTTAATTCAGGCGTGTC	300
		Sm_ter_4R	GGACGGTTGGACTTATTCCG	
	5	Sm_ter_5F	TTGTCCGTCTAAATAAGGTGTC	300
		Sm_ter_5R	TTGGACAAACTCAAACATGG	
	6	Sm_ter_6F	CACCGAATGATCAGGAATG	300
		Sm_ter_6R	GGTTTAAAAGCGAGAGACG	
	7	Sm_ter_7F	TTCCTTGTGGGTCTAATACTTG	300
		Sm_ter_7R	CAGAGCCATTAAGTAAATCACG	

	8	Sm_ter_8F	AGCATCAACACGTACGAAA	300
		Sm_ter_8R	GATTATCGGCATGAGACGG	
	9	Sm_ter_9F	GCGTAGGATTATTCTCATTAGC	314
		Sm_ter_9R	GGATAGCGCAAACGAGAAA	
<i>C. steedae ori</i> region (7,353 nt)	1	C_Ori1F	TCAATTTCAAAAACCGGCTC	300
		C_Ori1R	GATAGAACACATTATGTCTGCG	
	2	C_Ori2F	GCATGAGTGTGAAAGTAGC	300
		C_Ori2R	AAAAACCTGTGCATTCCAG	
	3	C_Ori3F	AACTGTGGTGTTC AACGTTA	300
		C_Ori3R	AGTTTGCCTTTCAGTTCAG	
	4	C_Ori4F	GTAGCCACGGTTCATTGA	331
		C_Ori4R	ACCACTTAGCCTAATTATCGG	
	5	C_Ori5F	AGGTTAAACAGTCAGTGGTAG	300
		C_Ori5R	TTTTTCGATCAAAGACGGG	
	6	C_Ori6F	TTTACCGAGCAATATGTCG	300
		C_Ori6R	GCGTACAAAGCGGTTAATC	
	7	C_Ori7F	GTGGTGCTGATTTACGATGA	300
		C_Ori7R	CAGACGTTGACTCAATGTG	
	8	C_Ori8F	GCGTCCCACGGATAATTAAT	300
		C_Ori8R	CGAATATTACGCCAACGAAAG	
	9	C_Ori9F	GCTTACCATACCTTCAAGC	300
		C_Ori9R	CGGCAAAAAGAAAAGTTTGAG	
	10	C_Ori10F	GTTAGACATAAACCCGACATGA	300
		C_Ori10R	CACCATGCTACTTGGTCTG	
	11	C_Ori11F	AGAAAGGAAACCCCATGTC	300
		C_Ori11R	GATTAAAGGTGGTAAATTCGCG	
<i>C. steedae ter</i> region (4,498 nt)	1	C_Ter1F	TTGCCCGACAACATTACTAC	300
		C_Ter1R	CTGTTTTCGGTTCATATAGG	
	2	C_Ter2F	GAAGGTTTTGAACGCATTCA	300
		C_Ter2R	CGAACTTTACACCTTTCCTTC	
	3	C_Ter3F	CGTAGATTTAAACGCTGACCT	300
		C_Ter3R	TAAGCCATTTCCCACTCG	
	4	C_Ter4F	GCCGACAGTATTTGCTTAC	300
		C_Ter4R	CTTTGTGTTGCCCGATATAATC	
	5	C_Ter5F	CCAAAGAGCAACTGGGTAT	300
		C_Ter5R	TGTCCAGTTGAAAATCTTCC	
	6	C_Ter6F	GCTTACCTTATTAGATGTGG	300
		C_Ter6R	GTAGGTTTTGTAGGGCTTT	
	7	C_Ter7F	GGTGGCGTATTGCTTAACT	300
		C_Ter7R	GTGTAAAGGTTCTAAATGGGAC	
	8	C_Ter8F	ACACCTTTTTATCGGTAGC	300
		C_Ter8R	TCGTCAAGGGGAATATCAG	

	9	C_Ter9F	AACAATGTGGACAAGCACT	300
		C_Ter9R	TACTGTGGGGGTCTAGTTG	
	10	C_Ter10F	CGGAATTACAGGTATCACAAC	300
		C_Ter10R	CAAGATGTTCCCTTTAACCAGTG	
<i>C. steedae</i> plasmid (7,353 nt)	1	Cs_Plasmid1F	AAACTGACTGCCATAGTGC	300
		Cs_Plasmid1R	CCGTTACCATTCATGATGC	
	2	Cs_Plasmid2F	TAAAGGTTCTTTAGACACGG	300
		Cs_Plasmid2R	GAACATTTGGCTTATCGTTG	
	3	Cs_Plasmid3F	CGTACCAATTGCCACAAATATC	300
		Cs_Plasmid3R	TTATATGCCACAAAAGACGA	
	4	Cs_Plasmid4F	CCAATCGCCGTTATGTAAA	331
		Cs_Plasmid4R	GTAGATTTGTTGCAACCTTG	
	5	Cs_Plasmid5F	AATACCGCCAAAGCATGTA	300
		Cs_Plasmid5R	TGATTGGATGAGCCATTTGA	
	6	Cs_Plasmid6F	ATTGGTTGCGGTAACAGTAA	300
		Cs_Plasmid6R	GCATTATACCGAGCAAAAACC	
	7	Cs_Plasmid7F	GGTCGTTTTGATTAGACG	300
		Cs_Plasmid7R	CACCACAAAATACCTTCAG	
	8	Cs_Plasmid8F	TTTCTGTTTGTGTATCCGGT	300
		Cs_Plasmid8R	ATGATGGTTGGCACAAGTT	
	9	Cs_Plasmid9F	GCACCCATATAACAATTGCTT	300
		Cs_Plasmid9R	CCTGATGAAATACGAACGT	

The primers for the probes were produced by Microsynth. The template for the polynucleotide production was made through a colony touch-down PCR (Table 11) using the first primer and the last primer to achieve a sequence on which all probes are included. The amplicon size was verified using agarose gel electrophoresis, running it for 1 hour in a 1% agarose gel. The template was then purified with a NEB Monarch PCR clean up kit (NEB, T1030), diluted 1:100, and sent for sequencing to confirm that it was the target DNA sequence.

Table 11: PCR conditions for template production

98°C	98°C	63°C [- 0.3°C/cycle]	72°C	4°C
5 min	20 seconds	20 seconds	4 min	pause
x1	x31 cycles			x1

The polynucleotides were then produced by touch-down PCR (Table 12), and the amplicon size per probe was verified using agarose gel electrophoresis, running it for 1 hour in a 1% agarose gel. The samples were cleaned using the NEB Monarch PCR clean up kit (NEB, T1030), and 3 or more reactions per primer pair were pooled together to achieve a higher polynucleotide concentration.

Table 12: PCR conditions for probe synthesis

98°C	98°C	63°C [Δ -0.3°C]	72°C	4°C
5 min	20 seconds	20 seconds	30 seconds	pause
x1	x31 cycles			x1

Labeling

Following purification, the PCR products were chemically labelled with different dyes using the ULYSIS Alexa Fluor 594 nucleic acid labelling kit (Thermo Fisher, U21654). Firstly, the probe concentration was measured using Qubit. 100 ng/ μ l of each probe was added to a thin PCR tube and mixed. The probes were denatured at 95°C for 5 minutes in a thermocycler and then transferred directly to ice. The labelling reagent was added to the tube, 15 μ l of Alexa594 per 10 probes was utilized. It was incubated at 80°C for 30 minutes after which it was transferred to ice and centrifuged. Gel columns were utilized to purify the probes, and the samples were centrifuged to elute the labelled probes.

Direct-gene FISH:

For the full direct-geneFISH experiment, a modified version of the direct-gene FISH protocol (Barrero-Canosa et al., 2017) was followed.

Preparation of Buffers and Materials:

Lysozyme buffer

50 ml of lysozyme buffer was made by mixing 10X PBS (f.c. 1X), 0.5M EDTA (f.c. 0.05M), 1M Tris-HCl (f.c. 0.1M) and up to 50 ml of DEPC water.

Hybridization buffer

20 ml hybridization buffer was made by mixing in a conical centrifuge tube dextran sulfate (f.c. 20%), 45% (vol/vol) formamide, 20X SCC (f.c. 5X SCC), 5 M EDTA, pH 8.0 (f.c. 20 mM), and 4.1 ml of water. The tube was vortexed and then incubated in a water bath at 48°C until the dextran sulfate was completely dissolved. The solution was cooled to room temperature and then 10% blocking reagent (f.c. 1% wt/vol), sheared salmon sperm (f.c. 25 mg/ml), yeast RNA (f.c. 25 mg/ml), 100% formamide (f.c. 35%) and 20% SDS (f.c. 0.1% wt/vol). The solution was vortexed and filtered through a 0.22 μ m sterile syringe filter. It was aliquoted into 2 ml Eppendorf tubes and stored at -20°C. Before it was utilized for the experiment it was warmed up to 42°C.

Washing buffer

Washing buffer was prepared with 30mM NaCl, 5 mM EDTA, 20 mM Tris-HCl and 0.01% (wt/vol) SDS.

Permeabilization buffer

Permeabilization buffer was made by the addition of lysozyme to the lysozyme buffer at a concentration of 0.5 mg/mL.

Cell preparation:

Cell fixation

A culture of *S. muelleri* was grown to an OD₆₀₀ of 0.6 and a sample was fixed with 37% formaldehyde to reach a final concentration of 4% formaldehyde. It was incubated for 1 hour at room temperature before centrifugation for 10 minutes at 5000xg at 4°C. The supernatant was removed with care and the cell pellet was resuspended in 1X PBS. The cells were centrifuged for 10 minutes at 5000xg at 4°C, and the supernatant was again removed. Then 250 µl of 1X PBS was added, and 250 µl of 100% ethanol, and the cells were resuspended and stored at -20°C until used for FISH.

Cell immobilization

The epoxy slides were coated with poly-L-lysine. 50 µl of poly-L-lysine was placed on each well of the slide for 10 minutes, then it was removed and dried at 60°C for 20 minutes. 1 µl of fixed cells were spotted on slides and dried at 60°C in an oven. They were then dehydrated by immersion of the slide in falcon tubes containing 50%, 80% and 100% ethanol for 1 minute each and air-dried.

Cell permeabilization

100 µl of permeabilization solution was added to each well, and the slide was put into a sealed plastic box to avoid evaporation. It was placed at 37°C for 1 hour. The slides were transferred from the permeabilization solution into water for 1 minute, then ethanol for 1 minute using tweezers to move them. The slides were dried at 37°C.

Denaturation and Hybridization:

A humidity chamber was prepared by placing paper towels on the bottom of a glass box. The towels were soaked in 45% formamide solution, and a plastic tip rack was placed on top.

The hybridization mix was made by mixing hybridization buffer and the probe to a final concentration 50-200 pg/µl. 80 µl of hybridization mix was added to each well and the slides were placed in the humidity chamber and closed. The humidity chamber was placed in an oven at 85°C for 40 minutes then quickly moved to an oven at 46°C for 2 hours of hybridization.

During this time, the washing buffer was placed into a Schott bottle and incubated in a 48°C water bath.

The humidity chamber was opened in the chemical fume hood, and using tweezers, the slides were transferred to a Schott bottle with the warm washing buffer for a quick

wash of a few seconds followed by transfer to another bottle of washing buffer where it was incubated in a 48°C water bath for 15 minutes.

The slides were subsequently transferred to a Schott bottle with 1X PBS and incubated for 10 minutes at room temperature in the dark. PBS with 1:2000 dilution of Hoechst was prepared and spread over the wells, then incubated for 10 minutes in the dark. The slides were transferred to a falcon tube with water and incubated for 1 minute, after which they were dried at 37°C.

Counterstaining and mounting

1 µl of Vecta shield (Vector labs) was placed on the left side of each well. Then a coverslip was carefully placed on top. The borders of the coverslip were sealed with nail polish and air-dried, then the slide was ready for microscopy.

Microscopy and analysis

Cells subjected to Immunostaining and FISH were imaged using a Nikon Eclipse NI microscope equipped with a MFCool camera (Jenoptik). Images were acquired with ProgRes Capture Pro 2.8.8 software (Jenoptik). The images were analyzed using software ImageJ with plugin ObjectJ. Cell outlines for *A. filiformis* were automatically recognized and errors were removed manually. Cell outlines for *S. muelleri* and *C. steedae* were added manually. Cells were selected based on their phase-contrast images. Overlays were produced on ImageJ.

Results

Cell quantification of *A. filiformis*

OD₆₀₀ vs. DNA quantity

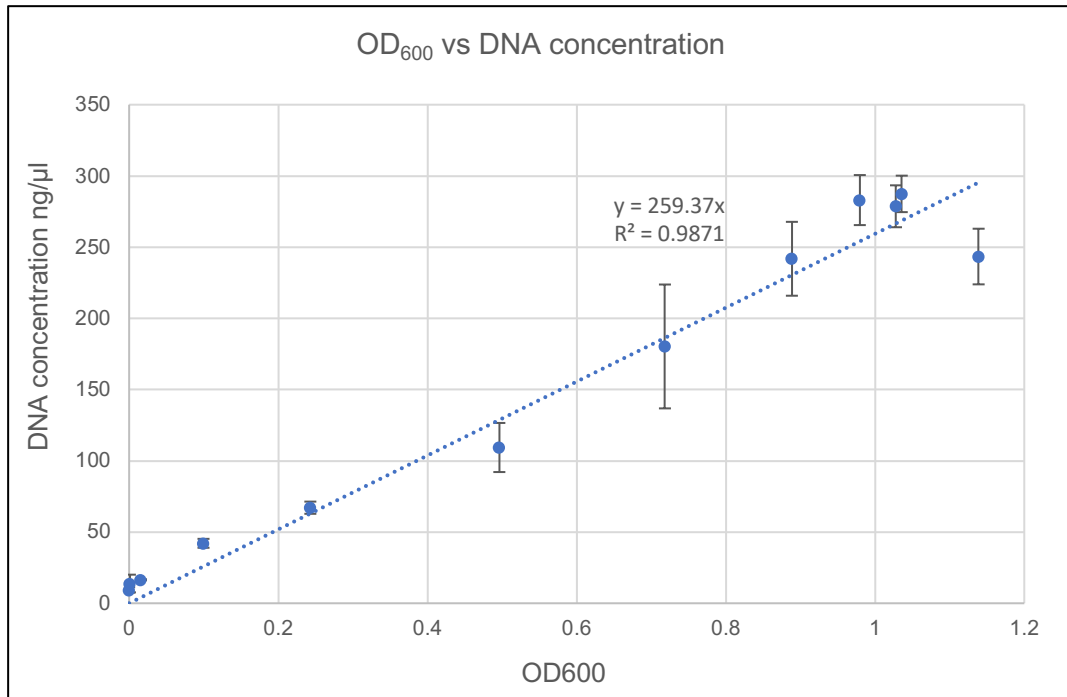


Figure 5. *OD₆₀₀* vs. DNA quantity. Every point represents the mean *OD₆₀₀*, and DNA concentration (ng/μl) of three independent biological replicates. Error bars represent standard deviation. The equation represents the line of best fit of the values.

The increase in *OD₆₀₀* correlates strongly with the increase in the quantity of DNA, as shown by the R^2 value of 98% (Figure 5). This correlation is expected because as the optical density increases it should signify that there are more copies of bacteria present, and thereby a higher DNA concentration.

Standards

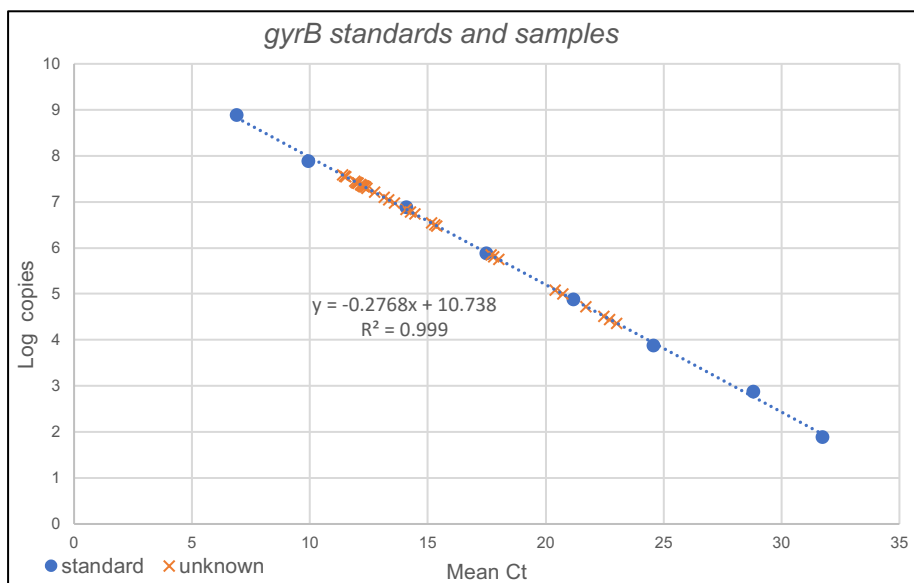


Figure 6. *gyrB* standards and samples. Mean Ct on the x-axis vs. log number of copies of *gyrB* on the y-axis. Every blue point represents a standard, and every orange value represents a sample. The equation represents the line of best fit of the standards.

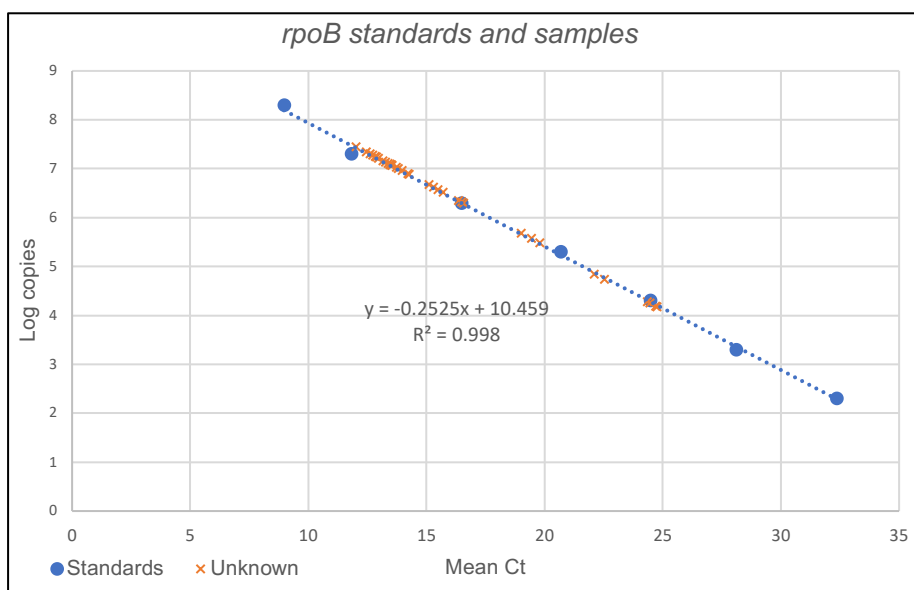


Figure 7. *rpoB* standards and samples. Mean Ct on the x-axis and log number of copies of *rpoB* on the y-axis. Every blue point represents a standard, and every orange value represents a sample. The equation represents the line of best fit of the standard samples.

The *gyrB* and *rpoB* samples all fall within the range of standard values (Figure 6, Figure 7, respectively). The R^2 values of 0.999 and 0.998 show that the standards strongly correlate linearly with log copies. The strong correlation indicates that the equations produced can be used for further calculations. Additionally, all the

unknowns fall within the standards showing that they are in the acceptable range. The negative controls also all fall below the standard values (not shown).

Copy number calculation

The number of copies in each sample is calculated with the equation produced in the standard graphs. Additionally, the sample was diluted twice, once during the plasmid extraction with 30 μ l and once during the qPCR sample dilutions by 4 μ l. Overall, this calculation will represent the total number of copies in 1 ml of culture.

Calculation for *gyrB* qPCR:

$$\text{Copies} = 10^{-0.2768x + 10.738} \times 30 \times 4$$

Calculation for *rpoB* qPCR:

$$\text{Copies} = 10^{-0.2525x + 10.459} \times 30 \times 4$$

Correlation

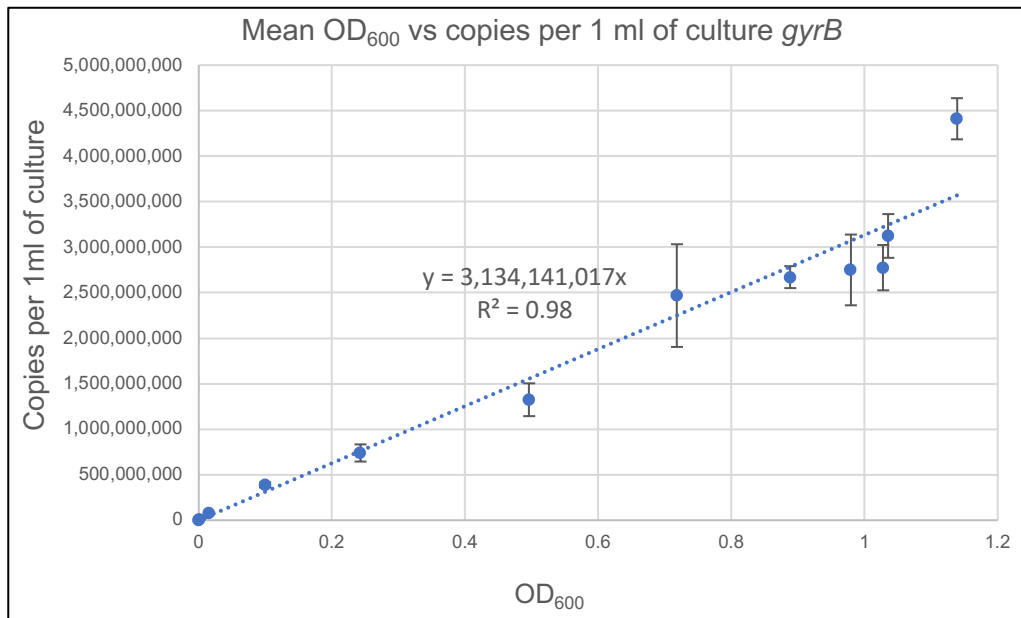


Figure 8. Mean OD₆₀₀ vs. copies per 1 ml of culture *gyrB*. Every point represents the OD₆₀₀ on the x-axis and the number of copies of *gyrB* per 1 ml of culture on the y-axis. Error bars represent standard deviation. The equation represents the line of best fit of the samples.

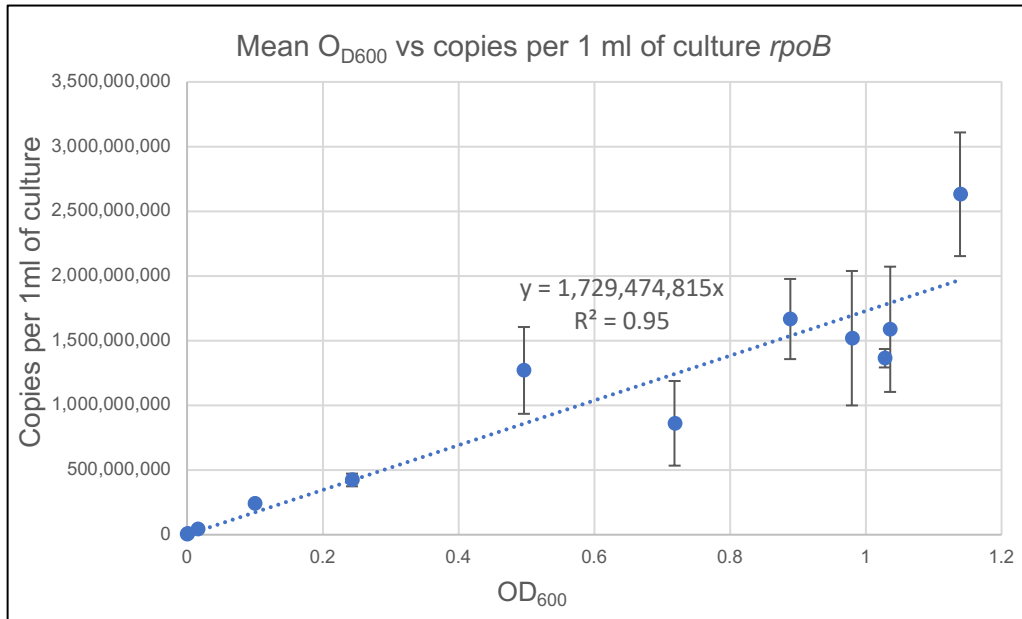


Figure 9. Mean OD₆₀₀ vs. copies per 1 ml of culture *rpoB*. Every point represents the OD₆₀₀ on the x-axis and the number of copies of *rpoB* per 1 ml of culture on the y-axis. Error bars represent standard deviation. The equation represents the line of best fit of the samples.

The relationship between OD₆₀₀ and copies of *rpoB* and *gyrB* per 1ml of culture both correlate strongly (Figure 8 and Figure 9, respectively). The R² values are both high, showing a strong correlation, however, the *gyrB* R² value is 0.98, while for *rpoB*, it is only 0.95. The relative standard error for *rpoB* ranged from 5%-54%, with a mean of 22.5%. The relative standard error for *gyrB* ranged from 5%-38%, with a mean of 12.7%. The relative standard deviation values for the *rpoB* graph values are significantly larger than the *gyrB* graph values meaning the results are not as precise for the *rpoB* qPCR. This may be due to the two weeks of time in between the two qPCRs, as the same DNA was utilized, and it may have degraded over that time. The DNA concentration was measured on the day of the *gyrB* qPCR and *rpoB* qPCR. The percentage change in DNA concentration over the two weeks ranged from 2% to 54%, with the median being 16.5%.

Additionally, the equations for the calculation of copies of cell per 1 ml of culture with the same OD₆₀₀ values are significantly different. For *gyrB* the equation for calculating the number of copies from OD₆₀₀ is $y = 3,134,141,017x$ and for *rpoB* it is $y = 1,729,474,815x$. At any given OD₆₀₀, the equation for *rpoB* would give approximately half the number of copies as the equation for *gyrB*.

Growth Rate and Doubling Time

The number of copies found was also utilized to determine the growth rate and doubling time of *A. filiformis*. The growth rate was calculated with the following equation. $N(t) = N_0 \times (1+r)^t$. Where r is the unknown growth rate, t is time passed, N_0 is initial number of cells and $N(t)$ is number of cells after time t .

The number of copies chosen was at hours 6 and 8, as this is during the exponential phase of the growth curve.

$$2405559301 = 483179977 \times (1+r)^2$$

$$r = 1.23$$

The growth rate for *A. filiformis* is 1.23.

The doubling time was calculated with the following equation. $Td = t \frac{70}{r}$. Td is doubling time and r is the growth rate in percentage.

$$Td = t \frac{70}{123}$$

$$Td = 1.15 \text{ hours}$$

The doubling time for *A. filiformis* is 69 minutes.

Morphometric Measurements

While the growth rate and doubling time are important basic knowledge of the bacteria, morphometric measurements are also key information. *A. filiformis* cells are the smallest overall. *C. steedae* cells are the longest out of the three, however, also the thinnest.

Table 13. Morphometric measurements

		<i>A. filiformis</i> (688 cells total)	<i>S. muelleri</i> (317 cells)	<i>C. steedae</i> (228 cells)
Length (µm)	Range	1.19-2.36	1.18-4.21	2.27-6.3
	Mean	1.91	2.72	4.89
Width (µm)	Range	0.47-1.89	0.144-2.84	0.26-2.27
	Mean	1.15	1.17	0.98

DNA localization in *S. muelleri* and *C. steedae* may be polar

S. muelleri

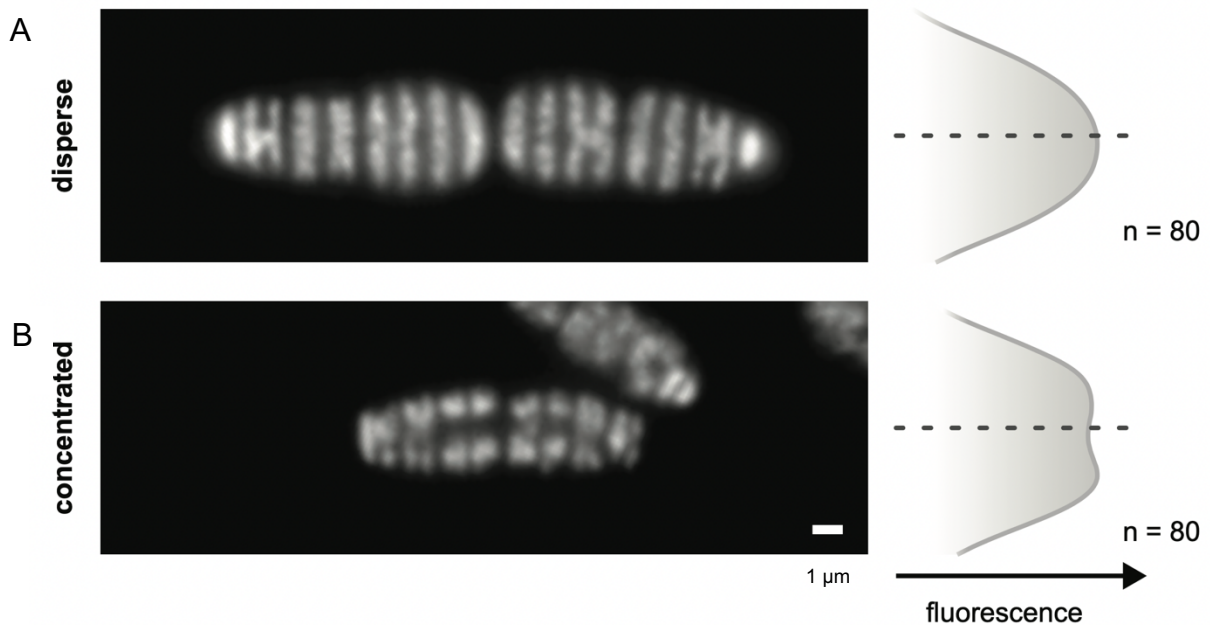


Figure 10. DNA localization in *S. muelleri*. (A) Microscopy image represents *S. muelleri* filaments stained using Hoechst 33343 and displaying a disperse DNA localization pattern, and the graph represents the distribution of signal measured along the length axis of the cells. (B) Microscopy image represents *S. muelleri* filaments stained using Hoechst 33343 and displaying a concentrated DNA localization pattern and the graph represents the distribution of signal measured along the length axis of the cells. Note that the DNA signal is excluded from the distalmost region of the cells. Scale bar 1 μm.

S. muelleri cells were stained with Hoechst 33342, and 160 cells were quantified. Two distinct DNA localization patterns are observed, disperse and concentrated (Figure 10). We qualified the DNA pattern as “disperse” if the DNA was spread evenly throughout the cell. There is no gap of fluorescent signal along the length of the DNA (Figure 10A graph). We qualified the pattern as “concentrated” when there was a gap in between two DNA-stained areas within the same cell, and the DNA localized towards the two host-attached poles (Figure 10B). The graph on the right shows a fall in fluorescent signal at the peak in the center of the cell.

C. steedae

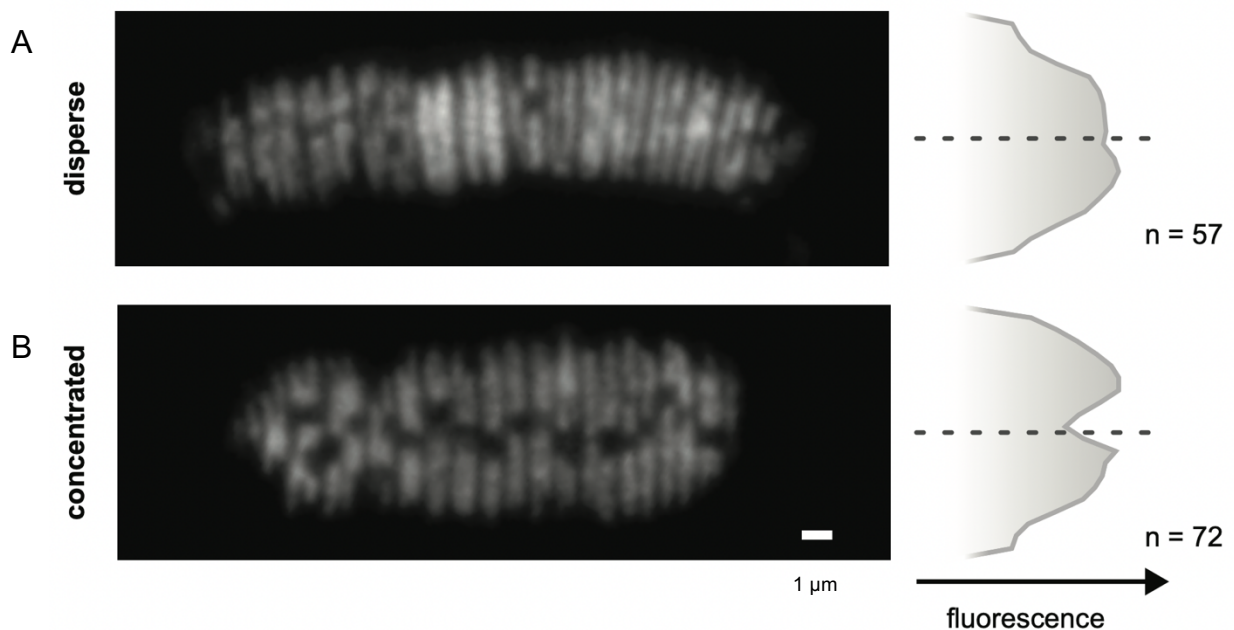


Figure 11. DNA localization in *C. steedae*. (A) Microscopy image represents *C. steedae* filaments stained using Hoechst 33342 and displaying a disperse DNA localization pattern, and the graph represents the spread of signal throughout the cells. (B) Microscopy image represents *C. steedae* filaments stained using Hoechst 3334 and displaying a concentrated DNA localization pattern, and the graph represents the spread of signal throughout the cells. Note that the DNA signal is excluded from the distalmost region of the cells. Scale bar 1 μm .

C. steedae cells were stained with Hoechst 33342, and 129 cells were quantified. Similarly to *S. muelleri*, two distinct DNA localization patterns are observed in these cells. 57 cells that were counted had DNA dispersed throughout the whole cell (Figure 11A), while 72 cells that were counted had more polar DNA, i.e., excluded from mid-cell which is the distalmost region of the cell (Figure 11B). The concentrated DNA pattern showed a gap in between two DNA areas in the center of the cell while the disperse DNA was spread evenly throughout the cell (Figure 11 graphs). Taken together, the DNA in *C. steedae* is present in two different patterns. Either dispersed throughout the cell equally or concentrated at either cell pole, leaving the mid-section, the most distal point, empty.

Detection of the tubulin homolog FtsZ was unsuccessful

Probing western blots of oral cavity symbiont protein extracts with a polyclonal anti-*C. crescentus* FtsZ antibody showed multiple bands, including two around 37 and 23 kDa for *C. steedae* and around 37 and 40 kDa for *A. filiformis* (Figure 12). For *S. muelleri* there was no band detected. The predicted size of the protein is 40 kDa. Despite multiple bands, the 37kDa and 40 kDa sized bands were the strongest. This signified that this antibody, although not specifically unless affinity purified, could detect the FtsZ protein within the cells.

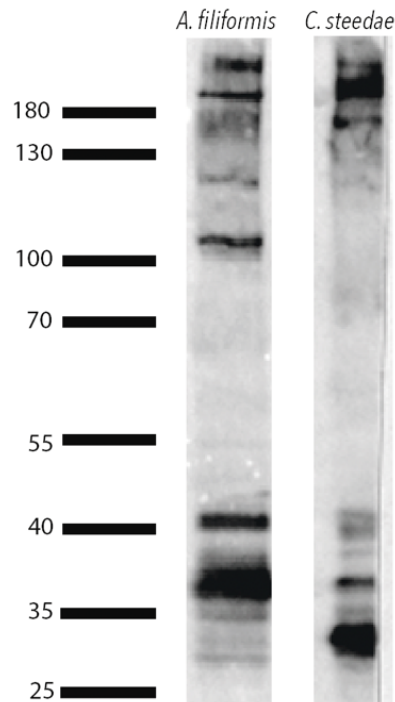


Figure 12. Western blot against FtsZ. Western blots of *A. filiformis* and *C. steedae* protein extracts probed with a polyclonal antibody against *C. crescentus* FtsZ. The marker indicating apparent molecular weights is expressed in kDa and is on the left.

Despite the fact that the protein bands detected on *A. filiformis* and *C. steedae* western blots could correspond to FtsZ, immunostaining with the anti-*C. crescentus* FtsZ antibody did not reveal the localization of the tubulin homolog. Unfortunately, cell permeabilization by using lysozyme led to the filaments breaking up into singular or double cells. On the other hand, without the use of lysozyme, the antibody appeared unable to enter the cell. Different lysozyme incubation times were tested (5 to 30 minutes). Additionally, multiple fixation methods were tried such as methanol, PFA, and ethanol. Furthermore, the cells were incubated with lysozyme after both drying on a slide and in Eppendorf tubes.

However, as of this point, no method proved to be optimal. The filaments were either broken up, making the signal location inconsistent, or the antibody seemed to be stuck on the outside of the cells (data not shown).

C. steedae fimbriae localization is polar

Ca. T. hypermnestrae, *A. filiformis* and *S. muelleri* are all vertically polarized, e.g., their fimbriae are exclusively localized to their host-attached regions. To find out whether *C. steedae* cells are also polarized, we immunostained cells with a commercially available antibody raised against *E. coli* fimbriae. The fimbriae signal clearly localized on the proximal, previously referred to as the ventral side (Pangborn, Kuhn & Woods, 1977) (Figure 13). This demonstrates the polarized nature of *C. steedae*, similar to *A. filiformis* and *S. muelleri* cell polarization previously shown in TEM images (Pangborn, Kuhn & Woods, 1977; Kaiser & Starzyk, 1973).



Figure 13. Polarized fimbriae localization in *C. steedae*. (A) Shows a phase-contrast image of a *C. steedae* filament. (B) Shows the same filament but with an overlay of two fluorescence signals. Magenta represents the DNA stained with Hoechst 33342 and green represents the anti-fimbriae antibody. Scale bar 5 μm.

Ori* are polar and *ter* are found at mid-cell in *S. muelleri

The *ori* and *ter* probes for DNA-FISH in *S. muelleri* all worked efficiently with little background signal. In *S. muelleri*, the *ori* foci are present at the two poles of the cell (Figure 14A). Moreover, more than one *ori* is found in most cells, one at each pole (Figure 14A). The view from the top of the cell demonstrates that the foci are mostly found on the two host-attached poles of the cell. Localization of *ori* foci of 188 cells resulted in heatmaps with two distinct clusters with a noticeable gap in between (Figure 14B). Additionally, most cells had two *ori* per cell (Figure 14C). More specifically, 47% of cells had two foci per cell or more (Figure 14C).

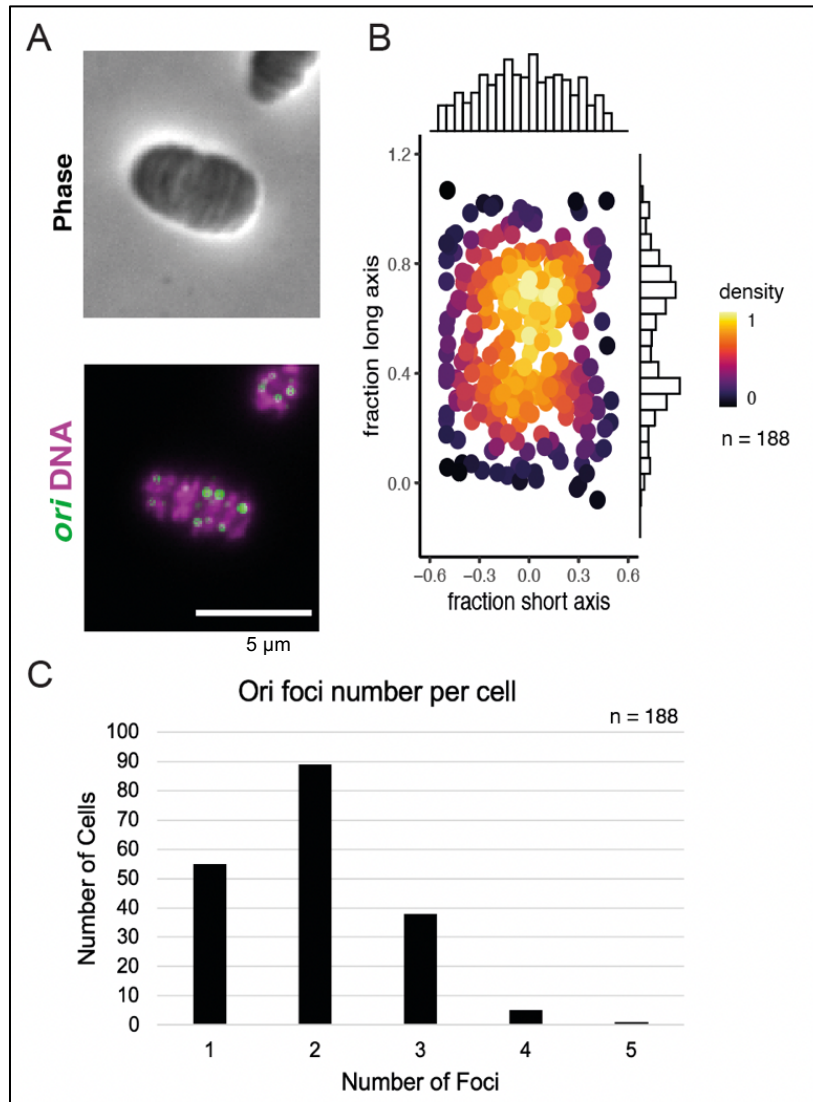


Figure 14. *ori* FISH experiment in *S. muelleri*. (A) The upper panel is a phase-contrast image, and the lower panel is an overlay of the two fluorescence signals, *ori* and DNA. Magenta represents the DNA stained with Hoescht 33342, and green represents the signal from *ori* FISH. (B) Heat map representing the highest density areas of the *ori* foci. (C) The number of foci per cell for the cells in which the *ori* was targeted by FISH. Scale bar 5 μm.

The *ter* foci signal is prevalent in the middle of the cell, also the most distal (furthest away) point from the host-attached poles (Figure 15A). Additionally, it was noticeable that some *ter* foci were larger than the *ori* foci. Analysis of 293 cells resulted in heat maps with a clear cluster of *ter* at mid-cell and absent from the poles (Figure 15B). For the *ter*, most cells had one focus but 30% of cells had two or more foci per cell (Figure 15C).

Overall, in *S. muelleri*, there are two *ori* per cell localized at the two cell poles and the *ter* is in the middle of the cell, and a high proportion of cells bear more than one *ori* focus.

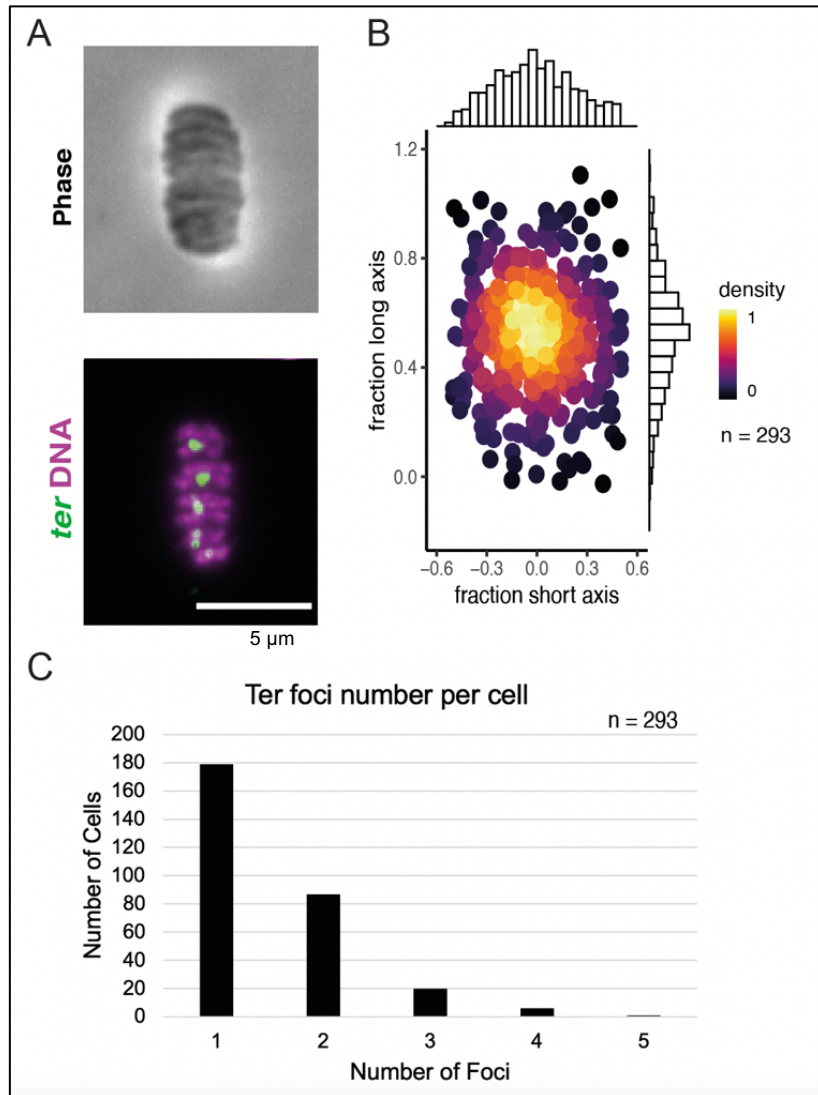


Figure 15. *ter* FISH experiment in *S. muelleri*. (A) The upper panel is a phase-contrast image, and the lower panel is an overlay of the two fluorescence signals, *ter* and DNA. Magenta represents the DNA stained with Hoescht 33342, and green represents the signal from *ter* FISH. (B) Heat map representing the highest density areas of the *ter* foci. (C) The number of foci per cell for the cells in which the *ter* was targeted by FISH. Scale bar 5 μm.

Ori* is polar and *ter* is found at mid-cell in *C. steedae

In *C. steedae*, similarly to *S. muelleri*, the *ori* foci are located at the two host-attached cell poles (Figure 16A). Analysis of 215 cells produced heat maps that demonstrate very distinctly the two areas where the *ori* are found, leaving the most distal area of the cell clear (Figure 16B).

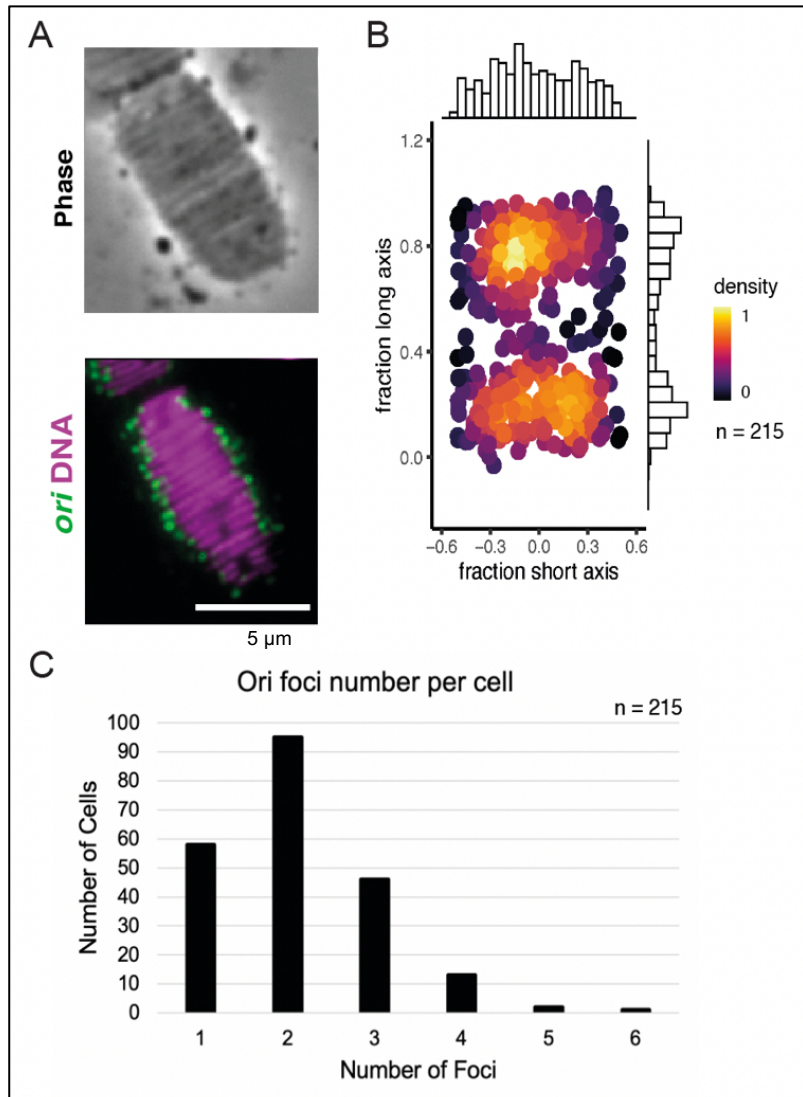


Figure 16. *ori* FISH experiment in *C. steedae*. (A) The upper panel is a phase-contrast image, and the lower panel is an overlay of the two fluorescence signals, *ori* and DNA. Magenta represents the DNA stained with Hoechst 33342, and green represents the signal from *ori* FISH. (B) Heat map representing the highest density areas of the *ori* foci. (C) The number of foci per cell for the cells in which the *ori* was targeted by FISH. Scale bar 5 μm.

The *ter*, as in *S. muelleri*, is most often in the middle of the cell (Figure 17A). Analysis of 236 cells produced heat maps demonstrating a strong clustering of the *ter* foci in the middle section of the cell, leaving the two poles empty (Figure 17B).

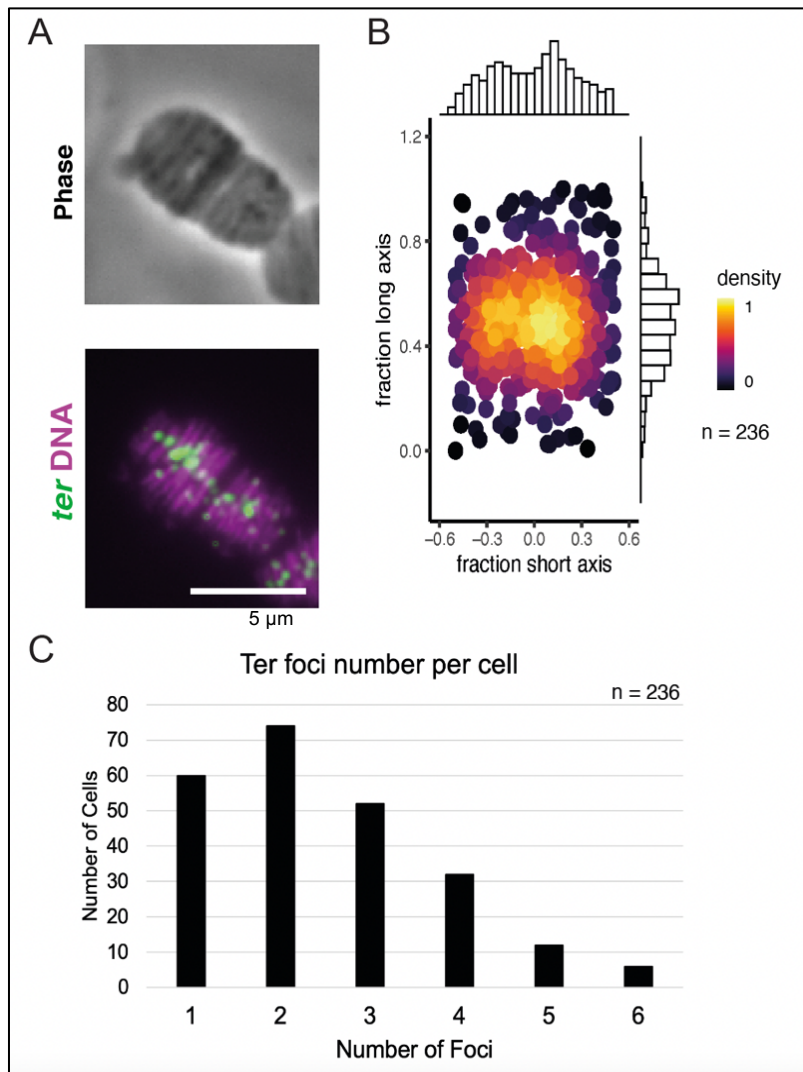


Figure 17. *ter* FISH experiment in *C. steedae*. (A) The upper panel is a phase-contrast image, and the lower panel is an overlay of the two fluorescence signals, *ter* and DNA. Magenta represents the DNA stained with Hoechst 33342, and green represents the signal from *ter* FISH. (B) Heat map representing the highest density areas of the *ter* foci. (C) The number of foci per cell for the cells in which the *ter* was targeted by FISH. Scale bar 5 μm.

Strikingly, for both the *ori* and *ter* of *C. steedae*, most cells have two foci. More specifically, 73% of the *ori* cells had two or more foci per cell, and 75% of the *ter* cells had two or more foci per cell. The cells with two foci also mostly have foci at the two opposite poles, signifying that there is more than one chromosome. Thereby, there is strong evidence that *C. steedae* is diploid.

Overall, in *C. steedae* there are two *ori* present in most cells, with one *ori* being at each cell pole, where the bacteria attach themselves to the host. The *ter* are in the center of the cell, the most distal point (furthest away) from the host attachment sites.

C. steedae plasmid localizes to the middle of the cell

The *C. steedae* large 80 kB plasmid (with lower copy numbers than the smaller *C. steedae* plasmid; T. Viehboeck, unpublished data) was the one targeted for this DNA-FISH. The plasmid signal is clearly localized in the middle area (between fraction long axis position 0.2 and 0.8) of the cell, leaving the poles vacant (Figure 18A). In the outer 1/5 of the cell, at both poles, there is very few foci found, as demonstrated by the heat map (Figure 18B).

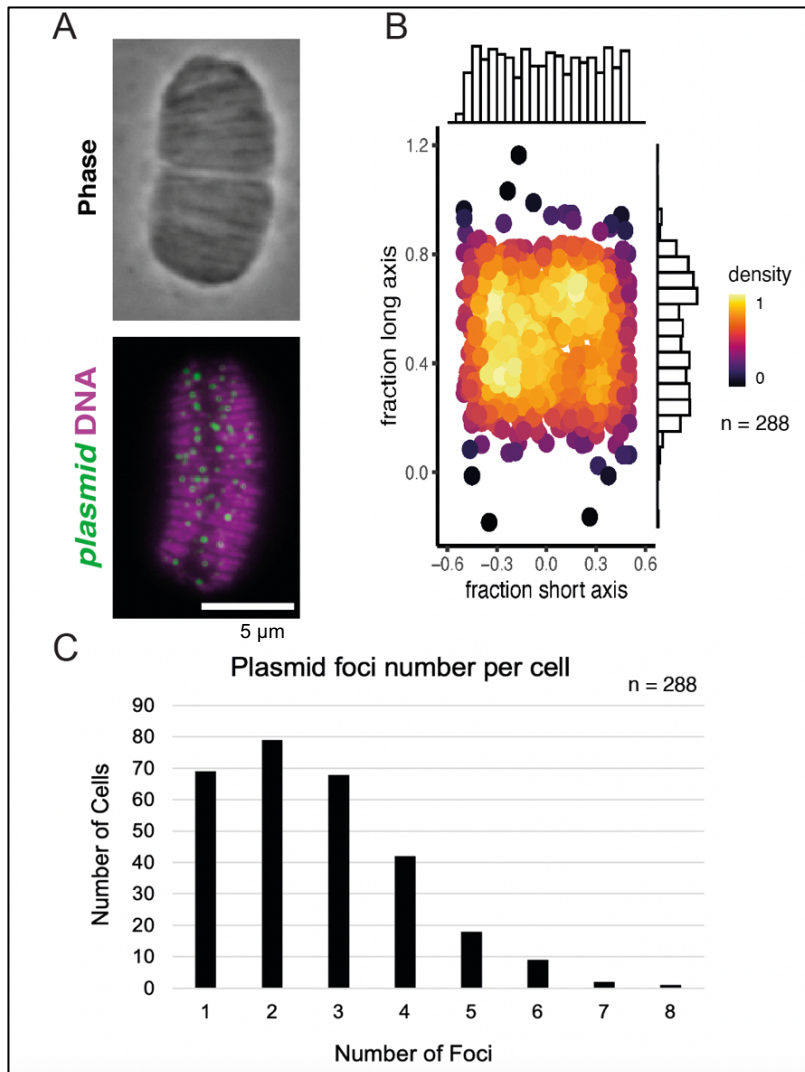


Figure 18. Plasmid FISH experiment in *C. steedae*. (A) The upper panel is a phase-contrast image, and the lower panel is an overlay of the two fluorescence signals, plasmid and DNA. Magenta represents the DNA stained with Hoechst 33342, and green represents the signal from plasmid FISH. (B) Heat map representing the highest density areas of the plasmid foci. (C) The number of foci per cell for the cells in which the plasmid was targeted by FISH. Scale bar 5 μm.

Discussion

Despite the prevalence of *A. filiformis*, *S. muelleri* and *C. steedae* in human oral cavities, there is a lack of investigations into their extraordinary cell biology. The methods to study chromosome configuration were first applied on nematode-attached symbionts *Ca. T. oneisti* and *Ca. T. hypermnestrae*, and their unusually stable chromosome configuration motivated the interest into studying more animal-attached symbiont chromosome configurations. The similarities in attachment to the animal host by polar fimbriae and longitudinal cell division (Weber et al., 2019) made the three oral cavity symbionts optimal candidates for the extension into this topic. Their ability to be cultivated easily in complex media allowed this study to make significant advances into knowledge surrounding animal-attached symbionts, not only in their chromosome configurations but also cell quantification, DNA localization, fimbriae localization and plasmid localization.

Cell quantification

Cell quantification is important for many studies involving *in vitro* bacterial cultures. Knowledge of the precise number of cells in each experiment ensures reproducibility and reliability. Traditional visual cell counting methods, such as cell counting with a hemocytometer, have not succeeded in counting multicellular filaments due to their unique morphology. The filaments often span through several grids, making it difficult to determine which grid the bacteria should be counted in. Automated cell counting methods such as flow cytometry require single cells, meaning the filaments must be separated, i.e., through sonication, which may lead to the loss of cells.

qPCR is a technique that monitors the amplification of a targeted DNA strand during PCR in real-time rather than at the final point as in a standard PCR. Previously, qPCR has been used to determine ploidy in bacteria by inputting a known number of cells and using a given single copy housekeeping gene as a proxy for the genome, i.e., the gene copy number corresponds to the genome copy number (Mendell et al., 2008). For single-copy genes, their number would equate to the number of bacteria in the sample. For example, *gyrB* and *rpoB* are two single copy housekeeping genes. *gyrB* plays an essential role in separating the DNA strands during DNA replication, while the *rpoB* gene forms a vital subunit of the RNA polymerase (Zaw, Emran & Lin, 2018).

Cell quantification of *A. filiformis* utilized qPCR to detect the number of copies at specific OD₆₀₀ values and resulted in understanding the bacteria's growth rate and doubling time. Certain experiments require accurate cell numbers, and as this has not been investigated in *A. filiformis* or related *S. muelleri* and *C. steedae* before, it was important to understand what volume of culture and which OD₆₀₀ was optimal for specific experiments.

The number of bacterial copies calculated for *rpoB* and *gyrB* was expected to be similar. Therefore, the mean copies between the two genes could be calculated and an equation could be produced, representing the number of bacteria in a sample. The number of copies calculated, however, varied greatly between the genes. *rpoB* copies at any given OD₆₀₀ value are almost half of the copies of *gyrB* with the same

OD600 value. While a slight difference was expected, this difference is too large to be considered reasonable.

When comparing the results of the *rpoB* and *gyrB* equations, there is a significant difference in relative standard error. The relative standard errors of *gyrB* correlated with the errors on the DNA concentration and OD₆₀₀, signifying that the errors on the *gyrB* figure are accounted for by the differing DNA concentrations due to the standard error in phenol-chloroform DNA extraction. For *rpoB*, it is evident that the larger relative standard error is not accounted for just by the method of DNA extraction. The *rpoB* qPCR was performed with the same samples approximately two weeks after the *gyrB* qPCR, meaning the samples underwent multiple freezing and thawing cycles during this time which often degrades DNA at a faster rate. The DNA degradation may account for the significant error bars present in the graph, and it also accounts for the decreased number of copies that were amplified during the qPCR for *rpoB*. In the future, this can be prevented by performing the qPCRs on the same day, with the same samples so that the DNA integrity does not impact the results. Additionally, the samples were stored in DEPC- H₂O, which does not preserve the DNA optimally like other options could, such as 50% glycerol-double-distilled water (Röder et al., 2010). Storage of the sample in alternative liquids may prevent the degradation if the qPCRs are unable to be performed on the same day. Furthermore, another single-copy gene may be tested to add to the accuracy of the bacterial copies per 1ml.

The smaller relative standard error and higher R² value of the *gyrB* data led to the conclusion that the *gyrB* data is more reliable than the *rpoB* data. Therefore, rather than combining them for a mean, the *gyrB* equation produced should be used for future calculations. This equation may be helpful for future studies in which the number of bacteria must be precise to produce reproducible and reliable results, such as FISH.

The growth rate and the doubling time were also calculated from the number of copies detected. The doubling time of 69 minutes is relatively similar to other bacteria in the *Neisseriaceae* family, for example, *Neisseria gonorrhoeae* has a doubling time of 90 minutes (Tobiason & Seifert, 2006). This data not only informs us about the quantity of *A. filiformis* at specific OD₆₀₀, but the method utilized for this can be applied for both *S. muelleri* and *C. steedae*. Future sampling of the bacteria from human oral cavities would also benefit as this quantification allows for evaluating human samples with specific primers.

Morphometric measurements

Previous morphometric measurements of *A. filiformis* concluded that the cells are 2-3 µm long and 0.6 µm wide (Radosavljevic et al., 2013), compared to the mean 1.91 µm long and 1.14 µm wide calculated in this study. While the length calculated here is shorter than the estimation established thus far, the width is larger.

Hedlund et al., concluded that *S. muelleri* cells are 1.9-6.4 µm long and 0.5-1.3 µm wide while Kuhn et al., concluded that they are 2.0-3.5 µm long and 0.5-0.9 µm wide (Hedlund, 2002; Kuhn & Gregory, 1978). When comparing these values to this study, we concluded that the cells are a mean of 2.72 µm long and 1.17 µm wide. While the

length of the cells corresponds to the ones previously published, the width found in this investigation seemed to be slightly larger.

C. steedae, previously known as *Simonsiella steedae*, was found to have a range of length from 2.5-7.1 μm (average 3.45 μm) and width of 0.7-1.3 (average 1.1 μm) (Kuhn & Gregory, 1978). Compared to this study which had a mean length of 4.89 μm and width of 0.98 μm , these values correlate strongly. The *C. steedae* values found in this study are comparable in width but slightly longer than the previous mean length.

The Fil-Tracer plugin utilized to measure the cells (Nyongesa, Weber et al., under revision: Nature Communications) works effectively for *A. filiformis* cells but does not adequately recognize the larger and crescent-shaped *S. muelleri* and *C. steedae* cells, signifying the cells must be measured manually. This resulted in a much lower number of cells being counted for *S. muelleri* and *C. steedae*.

The slight differences in size between the measurements in this study compared to previously published results may be related to their treatment with PFA during fixation and lysozyme during the FISH experiment. Additionally, the media used to grow the cells differs slightly in terms of solid plates, liquid media, and media components, resulting in different growth conditions. Overall, the morphometric measurements in this study and previous ones demonstrate that *A. filiformis* is the smallest bacteria of the three, and the one with the smallest difference in its length vs. width, making it more compact. *S. muelleri* cells are almost 1 μm longer than *A. filiformis*, but around the same width. *C. steedae* are significantly longer than both, almost 2 μm longer than *S. muelleri*, however, they are the thinnest species. Morphological measurements are important because, despite their differing sizes, the genome size of all three is similar, signifying that these dimensions may impact the chromosome biology of the bacteria.

Optimization of immunostaining protocol for FtsZ

Western blots probed with an antibody raised against *C. crescentus* FtsZ showed bands for *A. filiformis* and *C. steedae*. FtsZ is a tubulin homolog that assembles at the mid-cell and plays a role in bacterial cell division in many bacteria (Wang et al., 2020). Therefore, the localization of this protein within the cells would be beneficial in understanding the molecular mechanisms underlying the longitudinal division of the cells. Despite some bands detected on western blots probed with anti-FtsZ antibody, the tubulin homolog could not be detected by immunostaining.

A. filiformis and *C. steedae* form multicellular filaments, making it difficult to add a reagent that allows cell penetration without breaking up the filaments. A study by Springstein et al., investigated FtsZ and MreB immunostaining in multicellular cyanobacteria (Springstein et al., 2020). The study utilized two protocols, one with fixation on a slide and no use of lysozyme and one with fixation in a tube and the use of lysozyme. These worked for the multicellular cyanobacteria, however, did not function for *A. filiformis*. Upon fixation on the slide, the antibody did not enter the cell, and upon fixation with lysozyme the filaments broke up into single cells or double cells. The most promising combination was a result of fixing with PFA and adding lysozyme for 20 minutes on a slide. This allowed for specific foci to be visualized,

unlike other combinations during which only a smear of signal was seen (data not shown). Optimization of this protocol would first include minor alterations of the most promising combination of PFA fixation with 20 minutes of lysozyme on a slide and may be the key in optimizing the immunostaining protocol when targeting proteins within cells.

Improvements in the immunostaining protocol would be beneficial to analyze the localization pattern of proteins that may play a role in the cell division and chromosome configuration. For example, anti-FtsZ immunostaining may give insight into the longitudinal division of the bacteria, as was done in *Ca. T. oneisti*. The longitudinal membrane constriction of *Ca. T. oneisti* was concluded to be driven by FtsZ (Leisch et al., 2012). It forms Z-rings, a structure which the cell division machinery assembles. Then the divisome is formed, a structure made of proteins including FtsZ regulators that remodel and invaginate the membrane (Wang et al., 2020). MreB is associated with the regulation of the elongasome and appears to be essential for coordinating PG precursor synthesis. While these proteins are not directly associated with the chromosome configuration of the oral cavity symbionts, it is possible that the localization of FtsZ and MreB would be key features in understanding the assembly of cell division apparatus. Optimizing the immunostaining protocol would allow for the visualization of these proteins within the cells.

***C. steedae* and *S. muelleri* fimbriae and DNA localization are polar**

Despite the western blot with an anti-fimbriae antibody not producing any bands, immunostaining was still done on *C. steedae* as the antibody had worked on the phylogenetically related *A. filiformis* in the past and confirmed their polarity (Nyongesa, Weber et al., under revision: Nature Communications). The fimbriae were found only on the ventral side of the cells and were entirely absent on the dorsal side. Thus, *C. steedae* attach to the oral epithelia by their ventral side, which is also the concave area of the cells, similar to what was reported for *S. muelleri* (Hedlund & Tønjum, 2015).

Fimbriae mediate the recognition and adhesion of bacteria to their targets (Chandra et al., 2008). For example, *Salmonella* Type 1 fimbriae play an essential role in the initial infection stages during adhesion of the bacteria to host tissues (Chandra et al., 2008). In *E. coli*, suppression of Type 1 fimbriae completely inhibited biofilm formation (Rodrigues & Elimelech, 2009; Wang et al., 2018). Studies involving varying degrees of fimbriation showed that adhesion capabilities are significantly diminished along with fimbriae reduction (McLay et al., 2018). Moreover, the host and symbiont undergo extensive interactions during their lifespan, mostly through their attachment by the fimbriae. The polarity of the fimbriae suggests that the same cell area consistently localizes close to the host, possibly impacting chromosome configuration within the cell.

Furthermore, not only are the fimbriae polar but the DNA in *A. filiformis*, *S. muelleri* and *C. steedae* were found in two patterns, disperse or concentrated. The DNA was categorized as disperse when it was spread throughout the cell, whereas when the DNA was localized more polarly, leaving the most distal point in the cell-free, it was

categorized as concentrated. The concentrated pattern demonstrated the polar nature of the DNA within both *S. muelleri* and *C. steedae*.

The polar nature of the cell (as manifested by the polar localization of its fimbriae and, often, by its DNA) may impact chromosome conformation and configuration. Moreover, these bacteria were taken from liquid culture; they were not grown on agar plates or in oral cavities (their natural environment), yet they still maintained their polar nature. This implies that this is an intrinsic feature of the bacteria. The mechanisms for their polar characteristics are still unknown, with future investigations into this possibly giving more insight.

***S. muelleri* has a fixed chromosome configuration (*ori-ter-ter-ori*)**

Quantification of the *ori* foci localization showed that they were mostly found in the two host-attached poles of the cells, and the locations where the *ori* and *ter* were found were consistently the same. Upon closer look, it is clear that some foci are often overlapping, making the focus area of the *ter* larger than the *ori* foci. The mean foci size in *S. muelleri* in 12 cells with more than one *ter* foci is 0.35 μm , while in 12 cells with only one *ter* focus it is 0.56 μm . This may be because they are so close in space that the foci cannot be distinguished between each other. Nonetheless, the difference is striking when comparing the foci number to the same experiment done in *A. filiformis*. In *A. filiformis*, 97% of the cells for the *ori* and 95% of the cells for the *ter* were found to have one focus per cell, and the remaining percentage had two foci per cell. While *A. filiformis* is clearly monoploid, the 47% and 30% of cells in *S. muelleri* that had more than one *ori* and *ter*, respectively, demonstrates that *S. muelleri* is most likely diploid.

The chromosome configuration is reminiscent of one reported for the transversally dividing *C. glutamicum* (Böhm et al., 2017), and we will therefore refer to the *S. muelleri* chromosome configuration as fixed *ori-ter-ter-ori* (Figure 19): two chromosomes, both arranged in a longitudinal fashion, however, only taking up half of the cell length. This signifies that the *ori* are constantly held at the poles, which are located closest to the host, and the *ter* are at the most distal point, furthest from host-attached sites.

***C. steedae* has a fixed chromosome configuration (*ori-ter-ter-ori*)**

The *C. steedae* results further added to the findings of the *S. muelleri* chromosome configuration. The *ori* foci were found on the outer boundaries of the cell, at the edges of the Hoechst 33342 stained DNA. In *C. steedae*, the two *ori* clusters had a much clearer space between them at mid-cell when compared to *S. muelleri*. As mentioned earlier, *C. steedae* is almost double the length of *S. muelleri*, but thinner. This allows the *ori* foci to spread out more, and the heat maps show a clear distinction between the clusters. The *ter* foci also were found in the middle of the cell, at the most distal point. The *ori* are localized towards the two host attached poles, and the *ter* is at the point that is furthest from the host-attached pole.

In *C. steedae*, 73% of the *ori* cells had two or more foci per cell, and 75% of the *ter* cells had two or more foci per cell. For both *ori* and *ter*, most cells have two foci and 74% have three or four. If *C. steedae* was monoploid, at no point in the cell cycle

would there be three or four foci, possibly representing up to three or four chromosomes. However, if the cells were diploid, then most cells would have two chromosomes, and during the division stages of the cell cycle the chromosome number would increase to four, before the cell wall has divided.

The chromosome configuration predicted is the same as that of *S. muelleri*. A diploid bacterium, with the *ori* of each chromosome at one end and the *ter* of both in the middle (Figure 19). This configuration is longitudinal in a sense, however, the *ter* is not at the other pole, making it a deviation from the standard longitudinal. As in the case of *S. muelleri*, this chromosome configuration will be referred to as fixed *ori-ter-ori*, in analogy to the one reported for *C. glutamicum* (Böhm et al., 2017).

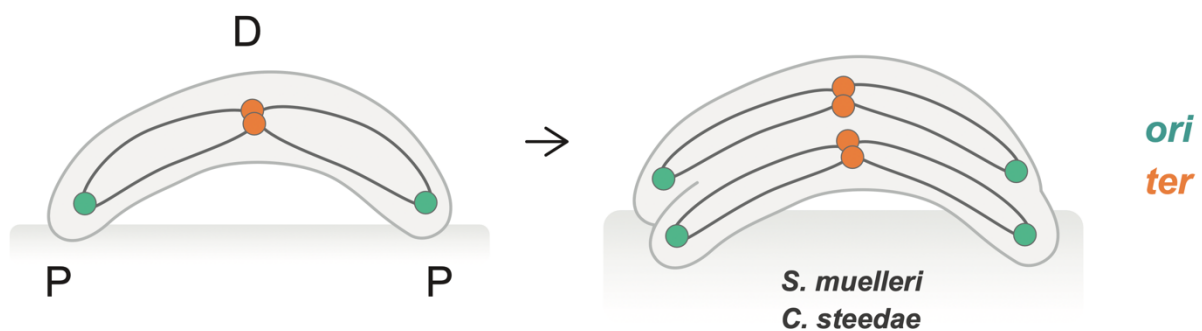


Figure 19. Diagram showing proposed chromosome configuration in *S. muelleri* and *C. steedae*. *ori* is green and *ter* is orange. D is distal and P is proximal. (Figure from Nyongesa, Weber et al., under revision: Nature Communications)

Diploidy

Although bacteria may be diploid (e.g., *C. glutamicum*), some *S. muelleri* and *C. steedae* cells had only one *ori* focus present. One reason for this could be that the foci seem to be overlapping in several cells, as shown by the larger size of the foci of the *ter* compared to the *ori*. Additionally, the efficiency of FISH is not 100%. Not every *ori* and *ter* were bound to the fluorescent probes and emitted a signal. This resulted in some cells clearly missing fluorescent signals and counted as having one focus only and some cells having no focus at all.

Occasionally, in fast-growing cells, a new round of replication begins before the previous round terminates, resulting in the so-called multifork replication (Youngren et al.). This results in newborn cells inheriting partially duplicated chromosomes with multiple *ori*. As we often saw multiple *ori* within a cell and less *ter*, a marker frequency analysis (MFA) (Galli et al., 2019) was performed to rule out the possibility that multiple *ori* were present due to the occurrence of multifork replication. MFA measures the ratio of *ori* to *ter*. If the ratio is 1:1 it would reflect that *S. muelleri* and *C. steedae* are diploid as the number of *ori* and *ter* are equal, however, if the number

of *ori* is higher than the number of *ter* it would demonstrate that multifork replication is occurring and the multiple *ori* per cell are due to multifork replication and not diploidy.

In *E. coli*, during stationary phase the ratio of *ori* to *ter* is 0.97, and in exponential phase, while multifork replication is occurring, the ratio is 2.5, meaning for every 2.5 *ori* there is one *ter* (Viehboeck, Weber et al., manuscript in preparation). For *A. filiformis*, the ratio during stationary phase is 1.5, and during exponential 1.7. For *S. muelleri* the ratio during stationary phase was 1.55, and during exponential 1.63. For *C. steedae* the ratio during stationary phase was 1.32, and during exponential 1.93 (Viehboeck, Weber et al., manuscript in preparation). The ratio at exponential phase of the oral cavity symbionts is much lower when compared to *E. coli*, a bacterium known to undergo multifork replication (Youngren et al., 2014). This allowed us to conclude that multifork analysis was likely not responsible for the multiple *ori*'s being visualized per cell with FISH.

Most bacteria appear to have a single large circular chromosome, making them monoploid. However, many prokaryotic species are polyploid, such as *Azotobacter vinelandii*, cyanobacteria (Soppa, 2021) and *C. glutamicum* (Böhm et al., 2017). Polyploidy offers a range of evolutionary advantages compared to monoploidy, such as resistance to conditions that induce double-stranded breaks and survival in harsher conditions (Soppa et al., 2014, Ludt, K and Soppa, 2019). The diploid nature of *S. muelleri* and *C. steedae* may have pushed the evolution of their unique chromosome configuration.

Fixed chromosome configuration

Most bacteria, including *E. coli*, constantly switch between longitudinal and transverse depending on cell cycle and environmental conditions (Wang & Rudner, 2014). However, *S. muelleri* and *C. steedae*, along with *A. filiformis*, *Ca. T. oneisti* and *Ca. T. hypermnestreae* all displayed chromosome configurations of unprecedented stability. A semi-fixed chromosome configuration, present in *Ca. T. oneisti*, can be defined as the chromosome maintaining its orientation towards the animal host transgenerationally, but presenting some dynamicity during DNA segregation (although *Ca. T. oneisti ori* stays at midcell, its *ter* moves from midcell to the poles back to midcell). Even more strikingly, a fixed chromosome configuration is present in *Ca. T. hypermnestreae*, *A. filiformis*, *S. muelleri* and *C. steedae*. This can be defined as the configuration being unchanged throughout all cell cycle stages and with respect to the animal host.

Furthermore, in *Ca. T. oneisti* it was hypothesized that the protein ParB was essential for *ori* localization. ParB immunostaining demonstrated that ParB co-localized with the *ori*. The ParABS system is commonly known for its role in several bacterial activities such as chromosome organization, gene expression and nucleoid occlusion, however, it often is not the only mechanism responsible for these processes (Sullivan, Marquis & Rudner, 2009; Gruber & Errington, 2009; Kadoya et al., 2011; Minnen et al., 2011). The co-localization of ParB with the *ori* in *Ca. T. oneisti* indicates that it plays a role in the chromosome configuration and segregation. In other polarized bacteria, such as *C. crescentus*, *ori* and ParB are tethered to the poles by a protein called PopZ (Holmes et al., 2016). However, no

known ParB anchors were found in the *Ca. T. oneisti* genome, thus, a yet unknown molecule may play a role in anchoring ParB and thus the chromosome in place (Weber et al., 2019). ParB may also play a role in tethering the chromosome to its specific location in *A. filiformis*, *S. muelleri* and *C. steedae*, and this may be further investigated with anti-ParB immunostaining. Furthermore, two polar bacteria that exhibit similarities to the oral cavity symbionts characteristics are *V. cholerae* and *C. crescentus*. They both divide utilizing the ParABS system (Jensen & Shapiro, 1999; Ramachandran, Jha & 2, 2014), making it possible that the polar *A. filiformis*, *S. muelleri* and *C. steedae* also utilize the ParABS system, which they all encode.

The fixed and semi-fixed chromosome configurations of the nematode-attached and oral cavity symbionts signify that the *ori* and *ter* are tethered to their positions by an unknown mechanism yet to be investigated, but possibly the ParABS system, given that they all possess the genetic repertoire to encode it (T. Viehboeck, Unpublished data)

C. steedae plasmid is excluded from the poles

The plasmid was localized around the center of the cell, absent from the cell poles, additionally highlighting *C. steedae* polarity. The plasmid stayed in the middle of the cell and was excluded from the most proximal 1/5 of the cell.

Plasmids are usually positioned to specific subcellular locations in a self-organizing manner (Hwang et al., 2013). In *E. coli*, different types of plasmids were all found to localize at mid-cell and quarter cell positions (Hwang et al., 2013). In bacteria containing more than one plasmid, such as *C. steedae*, each plasmid usually has its own specific position and mechanism for existence in a location within the cell (Ho, 2002). In addition, the plasmids within bacteria have mechanisms to tether themselves to specific locations (Mierzejewska & Jagura-Burdzy, 2012). Taken together, these characteristics all demonstrate the polarity of *C. steedae* which may play a role in the chromosome biology.

While the mechanism for the *C. steedae* plasmid positioning is still unidentified, the 80 kB plasmid encodes both a ParA and ParB protein, genes that are often encoded by many low copy plasmids (Bignell & Thomas, 2001). Some plasmids utilize tubulin or actin homologs to segregate newly replicated sister plasmids, but most low copy plasmids utilize the ParAB system for effective chromosome segregation (Sherratt, 2013). Considering the presence of *parA* and *parB* within the genome, it is highly likely that the *C. steedae* plasmid uses this system for plasmid segregation.

Concluding remarks

While the mechanism of tethering of the *ori* and *ter* to the poles is unknown, we can speculate about possible reasons why a fixed chromosome conformation would benefit animal-attached bacteria. Fixed chromosome configuration allows genetic loci to maintain the same intracellular position throughout the cell cycle. In the case of the oral cavity symbionts, this implies that genes adjacent to the *ori* will be closer to the host than genes adjacent to the *ter*. Which genes are situated in the vicinity of the *ori* and in the vicinity of the *ter*?

Primarily, gene location along the chromosome has been shown to play a role in gene expression in bacteria. The spatial ordering of genes along a chromosome is conserved and may correlate with their temporal expression patterns and gradient of DNA superhelical density from *ori* to *ter* (Sobetzko, Travers & Muskhelishvili, 2012). The organization of a complete chromosome encodes a spatiotemporal program integrating DNA replication and gene expression (Sobetzko, Travers & Muskhelishvili, 2012). For example, in *Salmonella typhimurium*, it was shown that the *his* protein was expressed at different levels, depending on their location in the chromosome (Schmid & Roth, 1987). The biggest difference in expression was observed in rapidly growing cultures between genes located either closer to the *ori* or closer to the *ter*. Additionally, in *E. coli* it was observed that gene positioning along the chromosome is one of the many mechanisms of adaptation to rapidly changing environments. This occurs through modulation of gene expression, with the highest gene expression being closest to the *ori* (Sousa, de Lorenzo & Cebolla, 1997). Finally, in *E. coli*, highly expressed NAPs during optimal growth phases are positioned closer to the *ori* and genes for NAPs expressed during late growth stage are closer to the *ter*, implying that there is also a spatiotemporal gene expression pattern for NAPs throughout the cell cycle (Shen & Landick, 2019). These studies demonstrate that gene localization along the chromosome impacts gene expression, and the genes close to the *ori* may be expressed more.

The genes located close to the *ori* in *A. filiformis* include secretion systems, T5cSS and amino acid transporters (Figure 20A). In *S. muelleri*, genes close to the *ori* encode for T4SS and T4 pili (Figure 20B). In *C. steedae*, the genes close to the *ori* are T5aSS and T5cSS, components of transporters (Figure 20C) (Viehboeck, Weber et al., manuscript in preparation). Genes encoding for secretion systems and transporters could be involved in host-symbiont interaction, and their proximal positioning may favor the deployment of their products at the host-symbiont interface.

While undoubtedly the *ori* and *ter* are essential components of the chromosome, and their localization gives great insight, the remaining areas of the chromosome are also important. To assess to which extent the rest of the chromosome interacts with the *ori* and *ter*, conformation capture sequencing (3C) was performed on *A. filiformis* (Viehboeck, Weber et al., manuscript in preparation). 3C quantifies the frequency of interaction between any two genomic loci. In *A. filiformis*, following the sequencing and mapping of 1 million reads, it was clear that there are at least 12 chromosome interaction domains ranging in size from 30-580 kB. More importantly, there is one fixed loop containing the *ori* that is 170 kB long. This loop contains highly expressed genes, including genes for ribosomal proteins, t4 pili assembly protein (PilY1),

vitamin transporters and amino acid transporters. The loop persisted in cells treated with rifampicin and in different growth stages, including exponential or stationary, making it transcription and growth-phase independent.

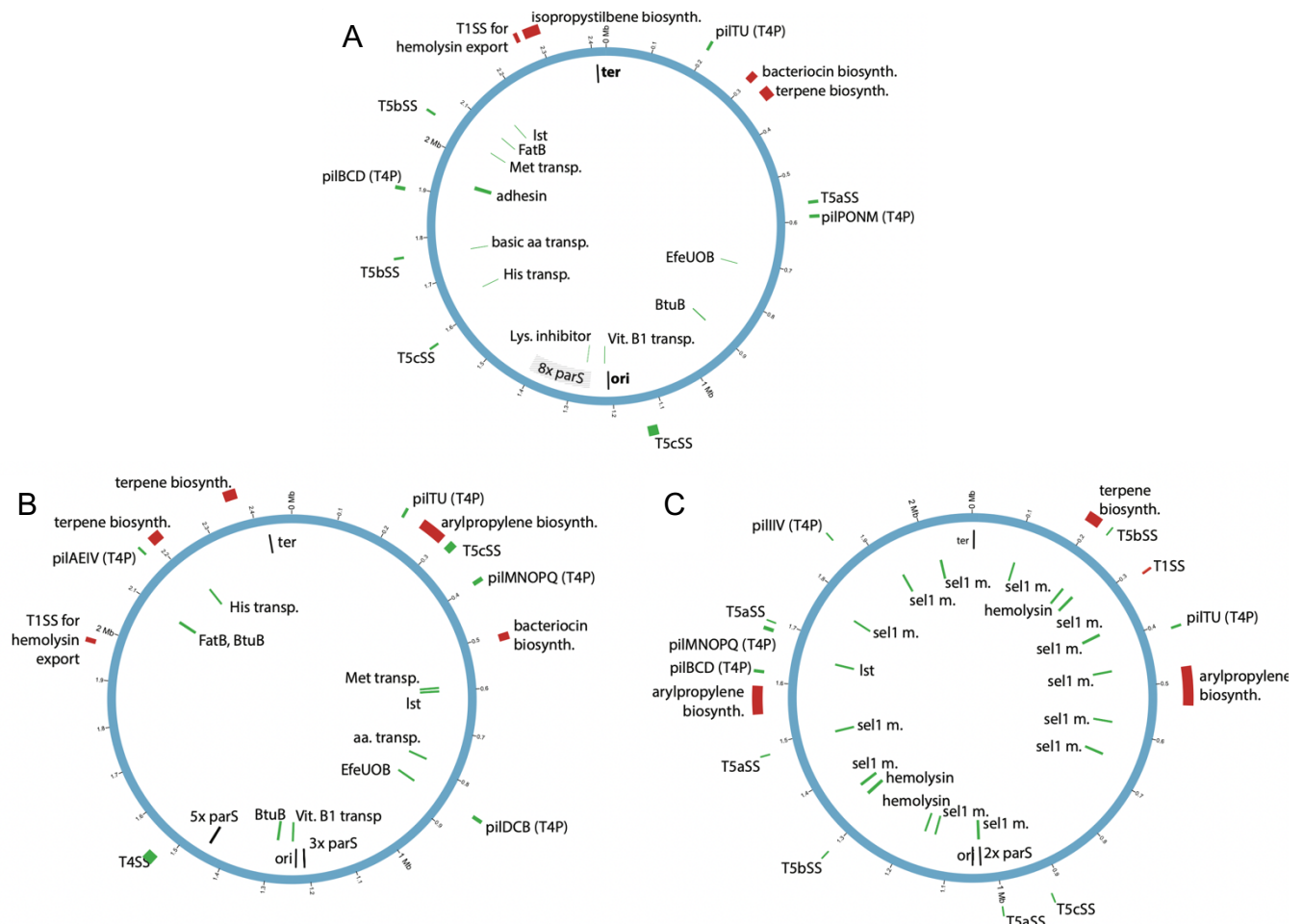


Figure 20. Genome maps of *A. filiformis*, *S. muelleri* and *C. steedae*. (A) Genetic position of selected genes putatively involved in host interaction (green) or antimicrobial defense (red) in *A. filiformis*. (B) Genetic position of selected genes putatively involved in host interaction (green) or antimicrobial defense (red) in *S. muelleri*. (C) Genetic position of selected genes putatively involved in host interaction (green) or antimicrobial defense (red) in *C. steedae*. *ori* is origin of replication. *ter* is terminus of replication. T1SS is type one secretion system. T4SS is type four secretion system. T5SS is type five secretion system. T4P is type four pili.

The location of the transporters within the *ori* loop may signify that they are highly expressed proteins with high abundance, but also that they are located close to the *ori* to be close to the host. The coordinated sharing of nutritional resources is one of the central features of symbiotic interactions, and transporters are essential for this (McDonald et al., 2021). The exchange of nutrients between the symbiont partner and the host partner would occur at the site of the transporters, which in this case is next to the *ori* and thus the one host attached pole in *A. filiformis* and two host attached poles in *S. muelleri* and *C. steedae*. Furthermore, the T4 pili assembly protein may be close to the *ori* because this is where the bacteria attach to their

hosts using their fimbriae. The location of *ori* to the host attached poles may be due to their symbiotic relationship with mammals and the necessity to transport vitamins and nutrients, such as vitamin B₁₂ which they cannot produce, from the host partner to themselves and vice versa. Further insight into the chromosome conformation of *S. muelleri* and *C. steedae* would be highly beneficial in understanding the loop around the *ori* in *A. filiformis*.

Outlook

This work has functioned to give major insights into *A. filiformis*, *S. muelleri* and *C. steedae*, however, much is left to elucidate. Their prevalence in the human population and presence in the oral cavity, an essential component of the human microbiome, make them vital bacteria to study. Knowledge into symbiotic bacteria ensures more accurate representations of bacteria *in vitro* and understanding of these bacteria may give insight into pathogenic bacteria, giving possible benefits to human health.

Confirmation of the diploidy of *S. muelleri* and *C. steedae* would be possible through differing methods. The simplest way to ensure the bacteria are diploid is to perform FISH targeting another area of the chromosome. A probe can be designed to target an area between the *ori* and *ter* and the number of foci per cell should be two if the cell is diploid. Moreover, if the probe were not close to the *ori* this method would avoid confusion with multifork replication. Additionally, performing *ori* targeting FISH on stationary phase cells would mean that all chromosomes are fully replicated. Thus, the number of foci per cell would be representative of the number of chromosomes without confusion with multifork replication. Another method to observe the number of foci per cell and to confirm the location of the *ori* would be immunostaining with ParB. ParB binds to *parS* sites that are generally located very close to the *ori* (Mierzejewska & Jagura-Burdzy, 2012). Thereby, the ParB fluorescent foci would highlight the location of the *ori*, and the number of foci per cell could give insight into the ploidy of the bacteria.

Immunostaining could not only give insight into the ploidy but also the role of certain proteins within the cell. Immunostaining with an anti-ParB antibody would demonstrate whether ParB plays a role in the tethering of the chromosome to its specific location. Furthermore, immunostaining with anti-FtsZ and anti-MreB would increase the knowledge surrounding the mechanism of longitudinal division of the bacteria. Overall, optimization of the immunostaining protocol for multicellular filaments with robust outer membranes could be key in understanding mechanistic features of cell growth in these oral cavity symbionts.

While 3C worked efficiently for *A. filiformis*, 3C is still in progress for *S. muelleri* and *C. steedae* (Viehboeck, Weber et al., manuscript in preparation). 3C will reveal which genetic loci, if any, physically interact with the *ori* and thereby are also localized close to the host. More globally, it will tell us whether the *ori*, or other regions of the chromosomes (e.g. the *ter*) are spatially isolated in macrodomains.

The fact that numerous genes potentially involved in symbiosis are adjacent to the *ori*, and the fact that this study revealed that the *ori* is invariably proximal suggests that the symbiont genome act as a master template that specifies the spatial localization of the transcription and translation as observed in *C. crescentus* (Montero Llopis et al., 2010). In this monoflagellated, vertically polarized bacterium mRNAs colocalize with the genes that generate them. This results in cells having the genes where they are needed. To confirm our hypothesis that the symbiont genome acts as a master template that dictates where genes are expressed, RNA FISH would be highly valuable.

References

- Aas, J.A., Paster, B.J., Stokes, L.N., Olsen, I. & Dewhirst, F.E. (2005) Defining the Normal Bacterial Flora of the Oral Cavity. *Journal of Clinical Microbiology*. 43 (11), 5721. doi:10.1128/JCM.43.11.5721-5732.2005.
- Abeles, A.L., Friedman, S.A. & Austin, S.J. (1985) Partition of unit-copy miniplasmids to daughter cells. *Journal of Molecular Biology*. 185 (2), 261–272. doi:10.1016/0022-2836(85)90402-4.
- Agnoli, K., Schwager, S., Uehlinger, S., Vergunst, A., Viteri, D.F., Nguyen, D.T., Sokol, P.A., Carlier, A. & Eberl, L. (2012) Exposing the third chromosome of *Burkholderia cepacia* complex strains as a virulence plasmid. *Molecular microbiology*. 83 (2), 362–378. doi:10.1111/J.1365-2958.2011.07937.X.
- Arweiler, N.B. & Netuschil, L. (2016) The Oral Microbiota. *Advances in Experimental Medicine and Biology*. 902, 45–60. doi:10.1007/978-3-319-31248-4_4.
- Barrero-Canosa, J., Moraru, C., Zeugner, L., Fuchs, B.M. & Amann, R. (2017) Direct-geneFISH: a simplified protocol for the simultaneous detection and quantification of genes and rRNA in microorganisms. *Environmental Microbiology*. 19 (1). doi:10.1111/1462-2920.13432.
- Bignell, C. & Thomas, C.M. (2001) The bacterial ParA-ParB partitioning proteins. *Journal of Biotechnology*. 91 (1), 1–34. doi:10.1016/S0168-1656(01)00293-0.
- Böhm, K., Meyer, F., Rhomberg, A., Kalinowski, J., Donovan, C. & Bramkamp, M. (2017) Novel Chromosome Organization Pattern in *Actinomycetales* —Overlapping Replication Cycles Combined with Diploidy. *mBio*. 8 (3). doi:10.1128/mBio.00511-17.
- Bonnefoy, E. & Rouvière-Yaniv, J. (1991) HU and IHF, two homologous histone-like proteins of *Escherichia coli*, form different protein-DNA complexes with short DNA fragments. *The EMBO Journal*. 10 (3), 687–696. doi:10.1002/j.1460-2075.1991.tb07998.x.
- Bonner, J.T. (1998) The origins of multicellularity. *Integrative Biology: Issues, News, and Reviews*. 1 (1). doi:10.1002/(SICI)1520-6602(1998)1:1<27::AID-INBI4>3.0.CO;2-6.
- Bright, M. & Bulgheresi, S. (2010) A complex journey: transmission of microbial symbionts. *Nature Reviews Microbiology*. 8 (3). doi:10.1038/nrmicro2262.
- Broyles, S.S. & Pettijohn, D.E. (1986) Interaction of the *Escherichia coli* HU protein with DNA. *Journal of Molecular Biology*. 187 (1), 47–60. doi:10.1016/0022-2836(86)90405-5.

- Chandra, H., Khandelwal, P., Khattri, A. & Banerjee, N. (2008) Type 1 fimbriae of insecticidal bacterium *Xenorhabdus nematophila* is necessary for growth and colonization of its symbiotic host nematode *Steinernema carpocapsiae*. *Environmental Microbiology*. 10 (5), 1285–1295. doi:10.1111/j.1462-2920.2007.01542.x.
- Chapple, I.L.C. & Genco, R. (2013) Diabetes and periodontal diseases: consensus report of the Joint EFP/AAP Workshop on Periodontitis and Systemic Diseases. *Journal of periodontology*. 84 (4 Suppl), S106–S112. doi:10.1902/JOP.2013.1340011.
- Chrostek, E., Pelz-Stelinski, K., Hurst, G.D.D. & Hughes, G.L. (2017) Horizontal Transmission of Intracellular Insect Symbionts via Plants. *Frontiers in Microbiology*. 8. doi:10.3389/fmicb.2017.02237.
- Deo, P.N. & Deshmukh, R. (2019) Oral microbiome: Unveiling the fundamentals. *Journal of Oral and Maxillofacial Pathology*. doi:10.4103/jomfp.JOMFP_304_18.
- Dethlefsen, L., McFall-Ngai, M. & Relman, D.A. (2007) An ecological and evolutionary perspective on human–microbe mutualism and disease. *Nature* 2007 449:7164. 449 (7164), 811–818. doi:10.1038/nature06245.
- Dewhirst, F.E., Chen, T., Izard, J., Paster, B.J., Tanner, A.C.R., Yu, W.-H., Lakshmanan, A. & Wade, W.G. (2010) The Human Oral Microbiome. *Journal of Bacteriology*. 192 (19). doi:10.1128/JB.00542-10.
- Dobell, C. (1920) The Discovery of the Intestinal Protozoa of Man. *Proceedings of the Royal Society of Medicine*. 13 (sect_hist_med), 1–15. doi:10.1177/003591572001301601.
- Douglas, A.E. (2009) Endosymbionts and Intracellular Parasites. *Encyclopedia of Microbiology*. 128–141. doi:10.1016/B978-012373944-5.00257-1.
- Egan, A.J.F. & Vollmer, W. (2013) The physiology of bacterial cell division. *Annals of the New York Academy of Sciences*. 1277 (1), 8–28. doi:10.1111/J.1749-6632.2012.06818.X.
- Funnell, B.E. (2016) ParB Partition Proteins: Complex Formation and Spreading at Bacterial and Plasmid Centromeres. *Frontiers in Molecular Biosciences*. 3. doi:10.3389/fmolb.2016.00044.
- Galli, E., Ferat, J.-L., Desfontaines, J.-M., Val, M.-E., Skovgaard, O., Barre, F.-X. & Possoz, C. (2019) Replication termination without a replication fork trap. *Scientific Reports*. 9 (1), 8315. doi:10.1038/s41598-019-43795-2.
- Gee, C.S., Pfeffer, J.T. & Suidan, M.T. (1990) *Nitrosomonas* and *Nitrobacter* Interactions in Biological Nitrification. *Journal of Environmental Engineering*. 116 (1), 4–17. doi:10.1061/(ASCE)0733-9372(1990)116:1(4).

- Gogou, C., Japaridze, A. & Dekker, C. (2021) Mechanisms for Chromosome Segregation in Bacteria. *Frontiers in Microbiology*. 12. doi:10.3389/fmicb.2021.685687.
- Gordon, B.R.G., Li, Y., Cote, A., Weirauch, M.T., Ding, P., Hughes, T.R., Navarre, W.W., Xia, B. & Liu, J. (2011) Structural basis for recognition of AT-rich DNA by unrelated xenogeneic silencing proteins. *Proceedings of the National Academy of Sciences*. 108 (26), 10690–10695. doi:10.1073/pnas.1102544108.
- Gruber, S. & Errington, J. (2009) Recruitment of Condensin to Replication Origin Regions by ParB/SpooJ Promotes Chromosome Segregation in *B. subtilis*. *Cell*. 137 (4), 685–696. doi:10.1016/j.cell.2009.02.035.
- Hamada, S., Amano, A., Kimura, S., Nakagawa, I., Kawabata, S. & Morisaki, I. (1998) The importance of fimbriae in the virulence and ecology of some oral bacteria. *Oral Microbiology and Immunology*. 13 (3). doi:10.1111/j.1399-302X.1998.tb00724.x.
- Hammel, M., Amlanjyoti, D., Reyes, F.E., Chen, J.-H., Parpana, R., Tang, H.Y.H., Larabell, C.A., Tainer, J.A. & Adhya, S. (2016) HU multimerization shift controls nucleoid compaction. *Science Advances*. 2 (7). doi:10.1126/sciadv.1600650.
- Han, Y.W. & Wang, X. (2013) Mobile microbiome: oral bacteria in extra-oral infections and inflammation. *Journal of dental research*. 92 (6), 485–491. doi:10.1177/0022034513487559.
- Hedlund, B.P. (2002) Phylogeny of the genus *Simonsiella* and other members of the Neisseriaceae. *International Journal of Systemic and Evolutionary Microbiology*. 52 (4), 1377–1382. doi:10.1099/ijs.0.01952-0.
- Hedlund, B.P. & Kuhn, D.A. (2006) The Genera *Simonsiella* and *Alysiella*. In: *The Prokaryotes*. New York, NY, Springer New York. pp. 828–839. doi:10.1007/0-387-30745-1_38.
- Hedlund, B.P. & Tønjum, T. (2015) *Simonsiella*. In: *Bergey's Manual of Systematics of Archaea and Bacteria*. Wiley. pp. 1–12. doi:10.1002/9781118960608.gbm00983.
- Herren, J.K., Paredes, J.C., Schüpfer, F., Arafah, K., Bulet, P. & Lemaitre, B. (2014) Insect endosymbiont proliferation is limited by lipid availability. *eLife*. 3. doi:10.7554/eLife.02964.
- Ho, T.Q. (2002) Compatible bacterial plasmids are targeted to independent cellular locations in *Escherichia coli*. *The EMBO Journal*. 21 (7), 1864–1872. doi:10.1093/emboj/21.7.1864.
- Hollister, E.B., Gao, C. & Versalovic, J. (2014) Compositional and Functional Features of the Gastrointestinal Microbiome and Their Effects on Human Health. *Gastroenterology*. 146 (6), 1449–1458. doi:10.1053/j.gastro.2014.01.052.

- Holmes, J.A., Follett, S.E., Wang, H., Meadows, C.P., Varga, K. & Bowman, G.R. (2016) *Caulobacter* PopZ forms an intrinsically disordered hub in organizing bacterial cell poles. *Proceedings of the National Academy of Sciences*. 113 (44), 12490–12495. doi:10.1073/pnas.1602380113.
- Hospenthal, M.K., Costa, T.R.D. & Waksman, G. (2017) A comprehensive guide to pilus biogenesis in Gram-negative bacteria. *Nature Reviews Microbiology*. 15 (6), 365–379. doi:10.1038/nrmicro.2017.40.
- Hwang, L.C., Vecchiarelli, A.G., Han, Y.-W., Mizuuchi, M., Harada, Y., Funnell, B.E. & Mizuuchi, K. (2013) ParA-mediated plasmid partition driven by protein pattern self-organization. *The EMBO Journal*. 32 (9), 1238–1249. doi:10.1038/emboj.2013.34.
- Iniesta, A.A. (2014) ParABS System in Chromosome Partitioning in the Bacterium *Myxococcus xanthus*. *PLoS ONE*. 9 (1), e86897. doi:10.1371/journal.pone.0086897.
- Jensen, R.B. & Shapiro, L. (1999) The *Caulobacter crescentus* smc gene is required for cell cycle progression and chromosome segregation. *Proceedings of the National Academy of Sciences*. 96 (19), 10661–10666. doi:10.1073/pnas.96.19.10661.
- Joyeux, M. (2015) Compaction of bacterial genomic DNA: clarifying the concepts. *Journal of Physics: Condensed Matter*. 27 (38), 383001. doi:10.1088/0953-8984/27/38/383001.
- Jun, S. & Mulder, B. (2006) Entropy-driven spatial organization of highly confined polymers: Lessons for the bacterial chromosome. *Proceedings of the National Academy of Sciences*. 103 (33), 12388–12393. doi:10.1073/pnas.0605305103.
- Kadoya, R., Baek, J.H., Sarker, A. & Chattoraj, D.K. (2011) Participation of Chromosome Segregation Protein ParA1 of *Vibrio cholerae* in Chromosome Replication. *Journal of Bacteriology*. 193 (7), 1504–1514. doi:10.1128/JB.01067-10.
- Kaiser, D. (2003) Building a Multicellular Organism. <http://dx.doi.org/10.1146/annurev.genet.35.102401.090145>. 35, 103–123. doi:10.1146/ANNUREV.GENET.35.102401.090145.
- Kaiser, G.E. & Starzyk, M.J. (1973) Ultrastructure and cell division of an oral bacterium resembling *Alysiella filiformis*. *Canadian Journal of Microbiology*. 19 (3), 325–327. doi:10.1139/m73-054.
- Kennedy, B., Peura, S., Hammar, U., Vicenzi, S., Hedman, A., Almqvist, C., Andolf, E., Pershagen, G., Dicksved, J., Bertilsson, S. & Fall, T. (2019) Oral Microbiota Development in Early Childhood. *Scientific Reports 2019 9:1*. 9 (1), 1–14. doi:10.1038/s41598-019-54702-0.
- Kilian, M., Chapple, I.L.C., Hannig, M., Marsh, P.D., Meuric, V., Pedersen, A.M.L., Tonetti, M.S., Wade, W.G. & Zaura, E. (2016) The oral microbiome – an update for oral healthcare professionals. *British Dental Journal 2016 221:10*. 221 (10), 657–666. doi:10.1038/sj.bdj.2016.865.

- Kisner, J.R. & Kuwada, N.J. (2020) Nucleoid-mediated positioning and transport in bacteria. *Current Genetics*. 66 (2), 279–291. doi:10.1007/s00294-019-01041-2.
- Kobryn, K., Lavoie, B.D. & Chaconas, G. (1999) Supercoiling-dependent Site-specific Binding of HU to Naked Mu DNA. *Journal of Molecular Biology*. 289 (4), 777–784. doi:10.1006/jmbi.1999.2805.
- Krogh, T.J., Møller-Jensen, J. & Kaleta, C. (2018) Impact of Chromosomal Architecture on the Function and Evolution of Bacterial Genomes. *Frontiers in Microbiology*. 9. doi:10.3389/fmicb.2018.02019.
- Kuhn, D.A. & Gregory, D.A. (1978) Emendation of *Simonsiella muelleri* schmid and description of *Simonsiella steedae* sp. nov., with designations of the respective proposed neotype and holotype, strains. *Current Microbiology*. 1 (1), 11–14. doi:10.1007/BF02601699.
- Leewenhoeck, A. (1684) An abstract of a letter from Mr. Anthony Leevvenhoeck at Delft, dated Sep. 17. 1683. Containing some microscopical observations, about animals in the scurf of the teeth, the substance call'd worms in the nose, the cuticula consisting of scales. *Philosophical Transactions of the Royal Society of London*. 14 (159), 568–574. doi:10.1098/rstl.1684.0030.
- Leisch, N., Verheul, J., Heindl, N.R., Gruber-Vodicka, H.R., Pende, N., den Blaauwen, T. & Bulgheresi, S. (2012) Growth in width and FtsZ ring longitudinal positioning in a Gammaproteobacterial symbiont. *Current Biology*. 22 (19), R831–R832. doi:10.1016/j.cub.2012.08.033.
- Ley, R.E., Peterson, D.A. & Gordon, J.I. (2006) Ecological and evolutionary forces shaping microbial diversity in the human intestine. *Cell*. 124 (4), 837–848. doi:10.1016/j.cell.2006.02.017.
- Li, X., Kolltveit, K.M., Tronstad, L. & Olsen, I. (2000) Systemic Diseases Caused by Oral Infection. *Clinical Microbiology Reviews*. 13 (4), 547. doi:10.1128/CMR.13.4.547-558.2000.
- Lin, D.C.H., Levin, P.A. & Grossman, A.D. (1997) Bipolar localization of a chromosome partition protein in *Bacillus subtilis*. *Proceedings of the National Academy of Sciences of the United States of America*. 94 (9), 4721. doi:10.1073/PNAS.94.9.4721.
- Lioy, V.S., Cournac, A., Marbouty, M., Duigou, S., Mozziconacci, J., Espéli, O., Boccard, F. & Koszul, R. (2018) Multiscale Structuring of the *E. coli* Chromosome by Nucleoid-Associated and Condensin Proteins. *Cell*. 172 (4), 771-783.e18. doi:10.1016/j.cell.2017.12.027.
- Liu, Y., Chen, H., Kenney, L.J. & Yan, J. (2010) A divalent switch drives H-NS/DNA-binding conformations between stiffening and bridging modes. *Genes & Development*. 24 (4), 339–344. doi:10.1101/gad.1883510.

- Livny, J., Yamaichi, Y. & Waldor, M.K. (2007) Distribution of Centromere-Like *parS* Sites in Bacteria: Insights from Comparative Genomics. *Journal of Bacteriology*. 189 (23), 8693–8703. doi:10.1128/JB.01239-07.
- Lloyd-Price, J., Abu-Ali, G. & Huttenhower, C. (2016) The healthy human microbiome. *Genome Medicine*. 8 (1). doi:10.1186/s13073-016-0307-y.
- Lu, M., Xuan, S. & Wang, Z. (2019) Oral microbiota: A new view of body health. *Food Science and Human Wellness*. 8 (1), 8–15. doi:10.1016/J.FSHW.2018.12.001.
- Lucchini, S., Rowley, G., Goldberg, M.D., Hurd, D., Harrison, M. & Hinton, J.C.D. (2006) H-NS Mediates the Silencing of Laterally Acquired Genes in Bacteria. *PLoS Pathogens*. 2 (8), e81. doi:10.1371/journal.ppat.0020081.
- Lukaszczyk, M., Pradhan, B. & Remaut, H. (2019) The Biosynthesis and Structures of Bacterial Pili. *Sub-cellular Biochemistry*. In: pp. 369–413. doi:10.1007/978-3-030-18768-2_12.
- Lyons, N.A. & Kolter, R. (2015) On The Evolution of Bacterial Multicellularity. *Current Opinion in Microbiology*. doi:10.1016/j.mib.2014.12.007.
- Mackenzie, C., Simmons, A.E. & Kaplan, S. (1999) Multiple chromosomes in bacteria. The *yin* and *yang* of *trp* gene localization in *Rhodobacter sphaeroides* 2.4.1. *Genetics*. 153 (2), 525–538. doi:10.1093/GENETICS/153.2.525.
- Macvanin, M. & Adhya, S. (2012) Architectural organization in *E. coli* nucleoid. *Biochimica et Biophysica Acta (BBA) - Gene Regulatory Mechanisms*. 1819 (7), 830–835. doi:10.1016/j.bbagrm.2012.02.012.
- Manning, J., Dunne, E.M., Wescombe, P.A., Hale, J.D.F., Mulholland, E.K., Tagg, J.R., Robins-Browne, R.M. & Satzke, C. (2016) Investigation of *Streptococcus salivarius*-mediated inhibition of pneumococcal adherence to pharyngeal epithelial cells. *BMC Microbiology*. 16 (1), 225. doi:10.1186/s12866-016-0843-z.
- Marsh, P.D. (2000) Role of the oral microflora in health. *Microbial Ecology in Health and Disease*. 12 (3) pp.130–137. doi:10.1080/089106000750051800.
- McDonald, T.R., Rizvi, M.F., Ruitter, B.L., Roy, R., Reinders, A. & Ward, J.M. (2021) Posttranslational regulation of transporters important for symbiotic interactions. *Plant Physiology*. doi:10.1093/plphys/kiab544.
- McLay, R.B., Nguyen, H.N., Jaimes-Lizcano, Y.A., Dewangan, N.K., Alexandrova, S., Rodrigues, D.F., Cirino, P.C. & Conrad, J.C. (2018) Level of Fimbriation Alters the Adhesion of *Escherichia coli* Bacteria to Interfaces. *Langmuir*. 34 (3), 1133–1142. doi:10.1021/acs.langmuir.7b02447.
- Mendell, J.E., Clements, K.D., Choat, J.H. & Angert, E.R. (2008) Extreme polyploidy in a large bacterium. *Proceedings of the National Academy of Sciences of the United States of America*. 105 (18), 6730–6734. doi:10.1073/PNAS.0707522105.

- Mierzejewska, J. & Jagura-Burdzy, G. (2012) Prokaryotic ParA–ParB–parS system links bacterial chromosome segregation with the cell cycle. *Plasmid*. 67 (1), 1–14. doi:10.1016/j.plasmid.2011.08.003.
- Minnen, A., Attaiech, L., Thon, M., Gruber, S. & Veening, J.-W. (2011) SMC is recruited to oriC by ParB and promotes chromosome segregation in *Streptococcus pneumoniae*. *Molecular Microbiology*. 81 (3), 676–688. doi:10.1111/j.1365-2958.2011.07722.x.
- Mobley, H.L.T., Koch, A.L., Doyle, R.J. & Streips, U.N. (1984) Insertion and Fate of the Cell Wall in *Bacillus subtilis*. *JOURNAL OF BACTERIOLOGY*. 169–179.
- Mohl, D.A., Easter, J. & Gober, J.W. (2008) The chromosome partitioning protein, ParB, is required for cytokinesis in *Caulobacter crescentus*. *Molecular Microbiology*. 42 (3), 741–755. doi:10.1046/j.1365-2958.2001.02643.x.
- Montero Llopis, P., Jackson, A.F., Sliusarenko, O., Surovtsev, I., Heinritz, J., Emonet, T. & Jacobs-Wagner, C. (2010) Spatial organization of the flow of genetic information in bacteria. *Nature*. 466 (7302), 77–81. doi:10.1038/nature09152.
- Moran, N.A. (2006) Symbiosis. *Current Biology*. 16 (20). doi:10.1016/j.cub.2006.09.019.
- Mori, H., Kondo, A., Ohshima, A., Ogura, T. & Hiraga, S. (1986) Structure and function of the F plasmid genes essential for partitioning. *Journal of Molecular Biology*. 192 (1), 1–15. doi:10.1016/0022-2836(86)90459-6.
- Neu, J. & Rushing, J. (2011) Cesarean versus Vaginal Delivery: Long term infant outcomes and the Hygiene Hypothesis. *Clinics in perinatology*. 38 (2), 321. doi:10.1016/J.CLP.2011.03.008.
- Niki, H. & Hiraga, S. (1998) Polar localization of the replication origin and terminus in *Escherichia coli* nucleoids during chromosome partitioning. *Genes & Development*. 12 (7). doi:10.1101/gad.12.7.1036.
- van Noort, J., Verbrugge, S., Goosen, N., Dekker, C. & Dame, R.T. (2004) Dual architectural roles of HU: Formation of flexible hinges and rigid filaments. *Proceedings of the National Academy of Sciences*. 101 (18), 6969–6974. doi:10.1073/pnas.0308230101.
- Nyby, M.D., Gregory, D.A., Kuhn, D.A. & Pangborn, J. (1977) Incidence of *Simonsiella* in the oral cavity of dogs. *Journal of Clinical Microbiology*. 6 (1), 87–88. doi:10.1128/JCM.6.1.87-88.1977.
- Nyongesa S, Weber P, Bernet E, Pullido F, Neickarz M, Deaby M, Nieves C, Viehboeck T, Krause N, Rivera-Millot A, Nakamura A, Vischer N, VanNieuwenhze M, Brun Y, Cava F, Bulgheresi S, Veyrier F. (2022) Evolution of multicellular longitudinally dividing oral cavity symbionts (*Neisseriaceae*). *Under revision at nature communications*: <https://www.researchsquare.com/article/rs-1200288/v1>

Ott, J.A., Gruber-Vodicka, H.R., Leisch, N. & Zimmermann, J. (2014) Phylogenetic confirmation of the genus *Robbea* (Nematoda: Desmodoridae, Stilbonematinae) with the description of three new species. *Systematics and Biodiversity*. 12 (4), 434–455. doi:10.1080/14772000.2014.941038.

Oulhen, N., Schulz, B.J. & Carrier, T.J. (2016) English translation of Heinrich Anton de Bary's 1878 speech, 'Die Erscheinung der Symbiose' ('De la symbiose'). *Symbiosis*. 69 (3). doi:10.1007/s13199-016-0409-8.

de Pablo, P., Chapple, I.L.C., Buckley, C.D. & Dietrich, T. (2009) Periodontitis in systemic rheumatic diseases. *Nature reviews. Rheumatology*. 5 (4), 218–224. doi:10.1038/NRRHEUM.2009.28.

Pangborn, J., Kuhn, D.A. & Woods, J.R. (1977) Dorsal-ventral differentiation in *Simonsiella* and other aspects of its morphology and ultrastructure. *Archives of Microbiology*. 113 (3), 197–204. doi:10.1007/BF00492025.

Paredes, G. F. (2021) Omics-based Physiology of Marine Nematode Ectosymbioses. Department of Archaea Biology and Ecogenomics. University of Vienna.

Paredes, G.F., Viehboeck, T., Lee, R., Palatinszky, M., Mausz, M.A., Reipert, S., Schintlmeister, A., Maier, A., Volland, J.-M., Hirschfeld, C., Wagner, M., Berry, D., Markert, S., Bulgheresi, S. & König, L. (2021) Anaerobic Sulfur Oxidation Underlies Adaptation of a Chemosynthetic Symbiont to Oxic-Anoxic Interfaces. *mSystems*. 6 (3). doi:10.1128/mSystems.01186-20.

Patil, S., Rao, R., Amrutha, N. & Sanketh, D. (2013) Oral Microbial Flora in Health. *World Journal of Dentistry*. 4 (4), 262–266. doi:10.5005/JP-JOURNALS-10015-1242.

Pende, N., Wang, J., Weber, P.M., Verheul, J., Kuru, E., Rittmann, S.K.-M.R., Leisch, N., Van Nieuwenhze, M.S., Brun, Y. v., den Blaauwen, T. & Bulgheresi, S. (2018) Host-Polarized Cell Growth in Animal Symbionts. *Current Biology*. 28 (7), 1039-1051.e5. doi:10.1016/j.cub.2018.02.028.

Perera, M., Al-hebshi, N.N., Speicher, D.J., Perera, I. & Johnson, N.W. (2016) Emerging role of bacteria in oral carcinogenesis: a review with special reference to perio-pathogenic bacteria. *Journal of Oral Microbiology*. 8 (1), 32762. doi:10.3402/jom.v8.32762.

Pizarro-Cerdá, J. & Cossart, P. (2006) Bacterial Adhesion and Entry into Host Cells. *Cell*. 124 (4), 715–727. doi:10.1016/j.cell.2006.02.012.

Polz, M.F., Distel, D.L., Zarda, B., Amann, R., Felbeck, H., Ott, J.A. & Cavanaugh1, C.M. (1994) Phylogenetic Analysis of a Highly Specific Association Ectosymbiotic, Sulfur-Oxidizing Bacteria and a Marine Nematode between. *Applied and Environmental Microbiology*. 60 (12), 4461–4467.

Qian, Z., Zhurkin, V.B. & Adhya, S. (2017) DNA–RNA interactions are critical for chromosome condensation in *Escherichia coli*. *Proceedings of the National Academy of Sciences*. 114 (46), 12225–12230. doi:10.1073/pnas.1711285114.

- Qin, J., Li, R., Raes, J., Arumugam, M., Burgdorf, K.S., et al. (2010) A human gut microbial gene catalog established by metagenomic sequencing. *Nature*. 464 (7285), 59. doi:10.1038/NATURE08821.
- Radosavljevic, V., Zutic, J., Radanovic, O., Ivetic, V., Pavlovic, I. & Zutic, M. (2013) A Case Report: Isolation of *Alysiella filiformis* from Pig's Lungs. *Kafkas Universitesi Veteriner Fakultesi Dergisi*. doi:10.9775/kvfd.2013.8648.
- Ramachandran, R., Jha, J. & 2 (2014) Chromosome Segregation in *V. Cholerae*. *Journal of Molecular Microbiology and Biotechnology*. 24 (5–6), 360–370. doi:10.1159/000368853.
- Ramond, E., Maclachlan, C., Clerc-Rosset, S., Knott, G.W. & Lemaitre, B. (2016) Cell Division by Longitudinal Scission in the Insect Endosymbiont *Spiroplasma poulsonii*. *mBio*. 7 (4). doi:10.1128/mBio.00881-16.
- Rangarajan, A.A. & Schnetz, K. (2018) Interference of transcription across H-NS binding sites and repression by H-NS. *Molecular Microbiology*. 108 (3), 226–239. doi:10.1111/mmi.13926.
- Reyes-Lamothe, R., Nicolas, E. & Sherratt, D.J. (2012) Chromosome Replication and Segregation in Bacteria. *Annual Review of Genetics*. 46 (1), 121–143. doi:10.1146/annurev-genet-110711-155421.
- Reyes-Lamothe, R., Wang, X. & Sherratt, D. (2008) *Escherichia coli* and its chromosome. *Trends in Microbiology*. 16 (5), 238–245. doi:10.1016/j.tim.2008.02.003.
- Röder, B., Frühwirth, K., Vogl, C., Wagner, M. & Rossmannith, P. (2010) Impact of Long-Term Storage on Stability of Standard DNA for Nucleic Acid-Based Methods. *Journal of Clinical Microbiology*. 48 (11), 4260–4262. doi:10.1128/JCM.01230-10.
- Rodrigues, D.F. & Elimelech, M. (2009) Role of type 1 fimbriae and mannose in the development of *Escherichia coli* K12 biofilm: from initial cell adhesion to biofilm formation. *Biofouling*. 25 (5), 401–411. doi:10.1080/08927010902833443.
- Rossetti, V., Ammann, T.W., Thurnheer, T., Bagheri, H.C. & Belibasakis, G.N. (2013) Phenotypic Diversity of Multicellular Filamentation in Oral Streptococci. *PLoS ONE*. 8 (9). doi:10.1371/journal.pone.0076221.
- Round, J.L. & Mazmanian, S.K. (2009) The gut microbiota shapes intestinal immune responses during health and disease. *Nature Reviews Immunology*. 9 (5). doi:10.1038/nri2515.
- Russell, S.L., Chappell, L. & Sullivan, W. (2019) A symbiont's guide to the germline. *Current Topics in Developmental Biology*. doi:10.1016/bs.ctdb.2019.04.007.
- Sampaio-Maia, B. & Monteiro-Silva, F. (2014) Acquisition and maturation of oral microbiome throughout childhood: An update. *Dental Research Journal*. 11 (3), 291. doi:10.4103/1735-3327.135876.

Sato, S. (2021) Plasmodium—a brief introduction to the parasites causing human malaria and their basic biology. *Journal of Physiological Anthropology*. 40 (1), 1–13. doi:10.1186/S40101-020-00251-9/TABLES/1.

Schmid, M.B. & Roth, J.R. (1987) Gene location affects expression level in *Salmonella typhimurium*. *Journal of Bacteriology*. 169 (6), 2872–2875. doi:10.1128/jb.169.6.2872-2875.1987.

Shaevitz, J.W., Lee, J.Y. & Fletcher, D.A. (2005) *Spiroplasma* Swim by a Processive Change in Body Helicity. *Cell*. 122 (6), 941–945. doi:10.1016/j.cell.2005.07.004.

Shen, B.A. & Landick, R. (2019) Transcription of Bacterial Chromatin. *Journal of Molecular Biology*. 431 (20), 4040–4066. doi:10.1016/j.jmb.2019.05.041.

Sherratt, D. (2013) Plasmid partition: sisters drifting apart. *The EMBO Journal*. 32 (9), 1208–1210. doi:10.1038/emboj.2013.84.

Sobetzko, P., Travers, A. & Muskhelishvili, G. (2012) Gene order and chromosome dynamics coordinate spatiotemporal gene expression during the bacterial growth cycle. *Proceedings of the National Academy of Sciences*. 109 (2), E42–E50. doi:10.1073/pnas.1108229109.

re

Soppa, J. (2021) Non-equivalent genomes in polyploid prokaryotes. *Nature Microbiology* 2021. 1–3. doi:10.1038/s41564-021-01034-3.

Sousa, C., de Lorenzo, V. & Cebolla, A. (1997) Modulation of gene expression through chromosomal positioning in *Escherichia coli*. *Microbiology*. 143 (6), 2071–2078. doi:10.1099/00221287-143-6-2071.

Springstein, B.L., Weissenbach, J., Koch, R., Stücker, F. & Stucken, K. (2020) The role of the cytoskeletal proteins MreB and FtsZ in multicellular cyanobacteria. *FEBS Open Bio*. 10 (12), 2510. doi:10.1002/2211-5463.13016.

Starkenburg, S.R., Chain, P.S.G., Sayavedra-Soto, L.A., Hauser, L., Land, M.L., Larimer, F.W., Malfatti, S.A., Klotz, M.G., Bottomley, P.J., Arp, D.J. & Hickey, W.J. (2006) Genome Sequence of the Chemolithoautotrophic Nitrite-Oxidizing Bacterium *Nitrobacter winogradskyi* Nb-255. *Applied and Environmental Microbiology*. 72 (3), 2050–2063. doi:10.1128/AEM.72.3.2050-2063.2006.

STEED, P.A. (1962) *Simonsiellaceae* fam.nov.with characterization of *Simonsiella crassa* and. *Journal of general microbiology*. 29 (4), 615–624. doi:10.1099/00221287-29-4-615.

Sullivan, N.L., Marquis, K.A. & Rudner, D.Z. (2009) Recruitment of SMC by ParB-*parS* Organizes the Origin Region and Promotes Efficient Chromosome Segregation. *Cell*. 137 (4), 697–707. doi:10.1016/j.cell.2009.04.044.

- Tobiason, D.M. & Seifert, H.S. (2006) The Obligate Human Pathogen, *Neisseria gonorrhoeae*, Is Polyploid. *PLoS Biology*. 4 (6), e185. doi:10.1371/journal.pbio.0040185.
- Tønjum, T. (2015) *Alysiella*. *Bergey's Manual of Systematics of Archaea and Bacteria*. Wiley. pp. 1–5. doi:10.1002/9781118960608.gbm00973.
- Toro, E., Hong, S.-H., McAdams, H.H. & Shapiro, L. (2008) *Caulobacter* requires a dedicated mechanism to initiate chromosome segregation. *Proceedings of the National Academy of Sciences*. 105 (40), 15435–15440. doi:10.1073/pnas.0807448105.
- Typas, A., Banzhaf, M., Gross, C.A. & Vollmer, W. (2011) From the regulation of peptidoglycan synthesis to bacterial growth and morphology. *Nature Reviews Microbiology* 2012 10:2. 10 (2), 123–136. doi:10.1038/nrmicro2677.
- Ursell, L.K., Metcalf, J.L., Parfrey, L.W. & Knight, R. (2012) Defining the human microbiome. *Nutrition Reviews*. 70. doi:10.1111/j.1753-4887.2012.00493.x.
- Vecchiarelli, A.G., Neuman, K.C. & Mizuuchi, K. (2014) A propagating ATPase gradient drives transport of surface-confined cellular cargo. *Proceedings of the National Academy of Sciences*. 111 (13), 4880–4885. doi:10.1073/pnas.1401025111.
- Viehboeck T., Weber P., Krause N., Junier I., Varoquax N., Diallo B., Bocard F., Lioy V., and Bulgheresi S. Chromosome configuration in oral cavity symbionts. *manuscript in preparation*.
- Wang, L., Keatch, R., Zhao, Q., Wright, J.A., Bryant, C.E., Redmann, A.L. & Terentjev, E.M. (2018) Influence of Type I Fimbriae and Fluid Shear Stress on Bacterial Behavior and Multicellular Architecture of Early *Escherichia coli* Biofilms at Single-Cell Resolution. *Applied and Environmental Microbiology*. 84 (6). doi:10.1128/AEM.02343-17.
- Wang, M., Fang, C., Ma, B., Luo, X. & Hou, Z. (2020) Regulation of cytokinesis: FtsZ and its accessory proteins. *Current Genetics*. 66 (1), 43–49. doi:10.1007/s00294-019-01005-6.
- Wang, Q., Liu, J. & Zhu, H. (2018) Genetic and molecular mechanisms underlying symbiotic specificity in legume-rhizobium interactions. *Frontiers in Plant Science*. 9, 313. doi:10.3389/FPLS.2018.00313/BIBTEX.
- Wang, X. & Rudner, D.Z. (2014) Spatial organization of bacterial chromosomes. *Current Opinion in Microbiology*. 22. doi:10.1016/j.mib.2014.09.016.
- Weber, P.M., Moessel, F., Paredes, G.F., Viehboeck, T., Vischer, N.O.E. & Bulgheresi, S. (2019) A Bidimensional Segregation Mode Maintains Symbiont Chromosome Orientation toward Its Host. *Current Biology*. 29 (18), 3018-3028.e4. doi:10.1016/j.cub.2019.07.064.

West, S.A., Griffin, A.S., Gardner, A. & Diggle, S.P. (2006) Social evolution theory for microorganisms. *Nature Reviews Microbiology*. 4 (8), 597–607. doi:10.1038/nrmicro1461.

Youngren, B., Nielsen, H.J., Jun, S. & Austin, S. (2014) The multifork *Escherichia coli* chromosome is a self-duplicating and self-segregating thermodynamic ring polymer. *Genes & Development*. 28 (1), 71–84. doi:10.1101/gad.231050.113.

Zaw, M.T., Emran, N.A. & Lin, Z. (2018) Mutations inside rifampicin-resistance determining region of *rpoB* gene associated with rifampicin-resistance in *Mycobacterium tuberculosis*. *Journal of Infection and Public Health*. 11 (5), 605–610. doi:10.1016/j.jiph.2018.04.005.

Zhao, H., Chu, M., Huang, Z., Yang, X., Ran, S., Hu, B., Zhang, C. & Liang, J. (2017) Variations in oral microbiota associated with oral cancer. *Scientific Reports* 2017 7:1. 7 (1), 1–10. doi:10.1038/s41598-017-11779-9.